From Isotropic to Anisotropic Conductivities in P(NDI2OD-T2) by (Electro-)Chemical Doping Strategies

Yannic Gross, Daniel Trefz, Daniel Bauer, Carsten Dingler, Vishnu Vijayakumar, Viktoriia Untilova, Laure Biniek, Martin Brinkmann, Sabine Ludwigs

From Isotropic to Anisotropic Conductivities in P(NDI2OD-T_2) by (Electro-)Chemical Doping Strategies

Yannic M. Gross,[†] Daniel Trefz,[†] Daniel Bauer,[†] Carsten Dingler,[†] Vishnu Vijayakumar,[‡] Viktoriia Untilova,[‡] Laure Biniek,[‡] Martin Brinkmann,[‡] and Sabine Ludwigs[†,]*

[†]IPOC-Functional Polymers, Institute of Polymer Chemistry (IPOC), University of Stuttgart, Pfaffenwaldring 55, 70569 Stuttgart, Germany.

[‡]Institut Charles Sadron, CNRS – Université de Strasbourg, 23 rue du loess, 67034 Strasbourg, France.

E-mail: sabine.ludwigs@ipoc.uni-stuttgart.de

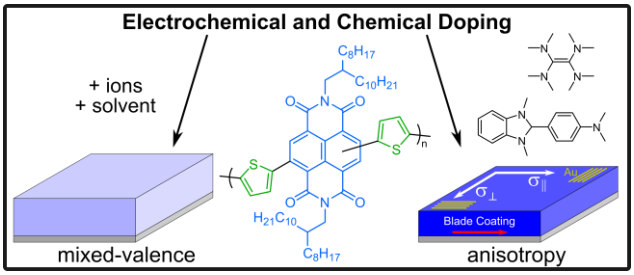

For Table of Contents use only.

Abstract.

New insights are given into the electrochemical and chemical doping behavior of the *n*-type regioregular polymer poly{[*N,N'*-bis(2-octyldodecyl)-naphthalene-1,4,5,8-bis(dicarboximide)-2,6-diyl]-*alt*-5,5'-(2,2'-bithiophene)} (P(NDI2OD-T_2)) and its regioirregular counterparts. Electrochemical experiments clearly show a two-fold reduction mechanism with maximum conductivity in the radical-anion state. Chemical doping with the high performance dopants N-DMBI and TDAE was studied and gives conductivity values between 10^{-4}–10^{-3} S cm^{-1} for as-cast films with clear involvement of the radical-anion species. Anisotropic conductivities of blade-coated films which were vapor doped give up to 6 times higher values along the polymer chain direction compared to the perpendicular direction, both in prominently face-on and edge-on oriented chains in the bulk of the films. The polymorph concomitantly changes from a mixed stacking of naphthalenediimide and bithiophene units (form II) to a segregated stacking mode (form I), indicating a strong effect of the dopant on the overall film structure. Maximum achievable conductivities along the chain are $8 \cdot 10^{-3}$ S cm^{-1}. Our study underlines that regardless of regioisomerism and film preparation higher maximum conductivity seem not to be achievable, at least with the here used chemical dopants. Reasons might include 1) the strong charge localization on the NDI units, 2) too low reduction potentials of the dopants used, 3) too high volatility of the dopants. The latter point is evidenced by transmission electron microscopy and electron diffraction experiments.

Introduction.

Inherently conducting polymers exhibit unique properties due to their conjugated backbones which can be reversibly oxidized or reduced. The search for both stable *n*-doped and *p*-doped systems with high conductivities is unbowed for applications such as thermoelectric generators or hole-blocking and electron-blocking layers for photovoltaic devices.[1–8] A thorough understanding in modifying and tuning of conductivities in organic semiconductors is needed and this is correlated to both backbone design and film morphology.[3,9,10] While p-type doping is rather well-studied in literature, n-type doping has only become an active field of research in the recent years due to a reduced number of available n-type polymer semiconductors prone to chemical or electrochemical n-doping.

Among different n-type polymers the semiconducting donor-acceptor polymer poly{[*N,N'*-bis(2-octyldodecyl)-naphthalene-1,4,5,8-bis(dicarboximide)-2,6-diyl]-*alt*-5,5'-(2,2'-bithiophene)} (P(NDI2OD-T_2)) is still one of the best performing systems and it can be regarded as the work-horse of the organic electronic community. The aggregating nature of P(NDI2OD-T_2) was highlighted by several reports in literature, and aggregation in solution together with the deposition technique are the key parameters for determining the performance in the final device.[11–14] A particularly straightforward experiment is simple blade coating which leads to extremely high anisotropies which can be explained by oriented fibers where the fiber direction coincides with the polymer chain direction.[15] The high aggregation tendency of P(NDI2OD-T_2) in organic solvents can be controlled by i) the choice of the solvent quality (which is difficult due to the poor solubility of the polymer, only 1-chloronaphthalene seems to be a good solvent) and ii) by introducing regioirregularity in the polymer backbone by copolymerization of 2,7- and 2,6-linked thiophene comonomers.[16,17]

It is commonly accepted that charge transport in semiconducting polymers is intrinsically anisotropic, being most effective along the chain and the π-stacking directions, as the solubilizing alkyl chains impede charge transport.[18–21] For P(NDI2OD-T_2) it was shown that anisot-

ropy in electron mobility is up to 20 with a favored transport along the polymer backbone.[20,22,23] While several studies have investigated the anisotropy of charge carrier in OFETs, the relation between chain orientation and bulk conductivity in doped *n*-type semiconducting polymers has not yet been addressed in details.[24]

Doping of conjugated polymer systems can in principle be done either electrochemically or chemically by external dopants. The reduction potential of P(NDI2OD-T_2) is –1.0 V vs. Fc/Fc^+, yielding a lowest unoccupied molecular orbital (LUMO) of ≈–4.1 eV, as measured by cyclic voltammetry.[25–27] The *n*-dopants therefore have to be strong electron donors with HOMO levels/ionization potentials with the same or higher energy level. Rather well-performing n-type external dopants include electron rich compounds such as dihydro-1*H*-benzoimidazol-2-yl derivatives[5,28] which had been successful for doping of fullerenes. In the case of fullerenes a probable reaction mechanism is a bimolecular hydride transfer from the hydride donor to the acceptor as the rate determining step, followed by an electron transfer between the reduced and unreduced fullerene.[29,30] Solution doping of P(NDI2OD-T_2) was mainly performed with dihydro-1*H*-benzoimidazol-2-yl derivatives like N-DMBI and N-DPBI yielding conductivities around $\sigma = 1-8 \cdot 10^{-3}$ S cm^{-1}.[28,31] In analogy to fullerenes, a hydride transfer is proposed,[30] however, clustering of the dopant on top of the film was found which leads to poor doping efficiencies of only 1 %.[28,32] Noteworthy, the reducing ability is not adequately described by HOMO/LUMO offsets and redox potentials, as the reduction is coupled with a chemical reaction.[30] A second explanation for the doping reaction could be the electron transfer from the neutral radical of N-DMBI after a hydrogen radical removal, which has an energy level of −2.36 eV (singly occupied molecular orbital SOMO energy calculated by Gaussian 03).[33] The SOMO has a higher energy than the LUMO of P(NDI2OD-T_2) (−4.1 eV), which could make reduction plausible.

Reducing vapors from branched poly(ethylene imine) or small molecule tetrakis(dimethylamino)ethylene (TDAE) have been investigated as alternative n-type do-

pants.[34,35] TDAE doping leads to maximum conductivities of around $5 \cdot 10^{-3}$ S cm^{-1} in P(NDI2OD-T_2) films. Recent studies on the host/dopant miscibility show enhanced conductivities for both fullerenes and naphthalenediimide copolymers with polar side chains.[32,36,37] Furthermore, it was proposed that in P(NDI2OD-T_2) an intrinsic limit around 10^{-3} S cm^{-1} is reached due to a strong localization of the doped state.[38]

In this contribution we bring new insights into the conductivity behavior of P(NDI2OD-T_2) with pure 2,6-linkage, i.e. the regioregular (RR) polymer, and mixed 2,6- and 2,7-linked isomers, the so-called regioirregular polymers, namely RI(70:30), RI (47:53) and RI(24:76), compare Scheme 1. In the first part pf this contribution, in-situ spectro-electrochemistry demonstrates that electrochemical redox doping occurs in two successive steps, from neutral via a radical-anion to a dianion species. Maximum conductivity is observed in the first reduction step, suggesting that charge transport is mainly via the radical-anion. In as-cast films of all polymers we also obtain the reduction to the radical-anion species in films upon chemical doping both with N-DMBI and TDAE. However, while the conductivity reaches values of 10^{-3} S/cm similar to literature, the intensity of the radical-anion band in absorption spectroscopy is surprisingly low. To gain further insight into this paradoxon we used TDAE vapor doping of films with well-defined oriented morphologies. Conductivity measurements evidence a high anisotropy of charge transport that is enhanced in direction of the polymer chain with anisotropy ratios up to a factor of 6. Absorption spectroscopy and transmission electron microscopy /electron diffraction give strong evidence for the volatility of TDAE dopant molecules that leave the films when removing the films from the vapor of the dopant, leaving a marginally doped film whose structure is substantially modified after the doping/dedoping processes.

Results and Discussion.

Influence of Regioregularity on Electrochemical Doping.

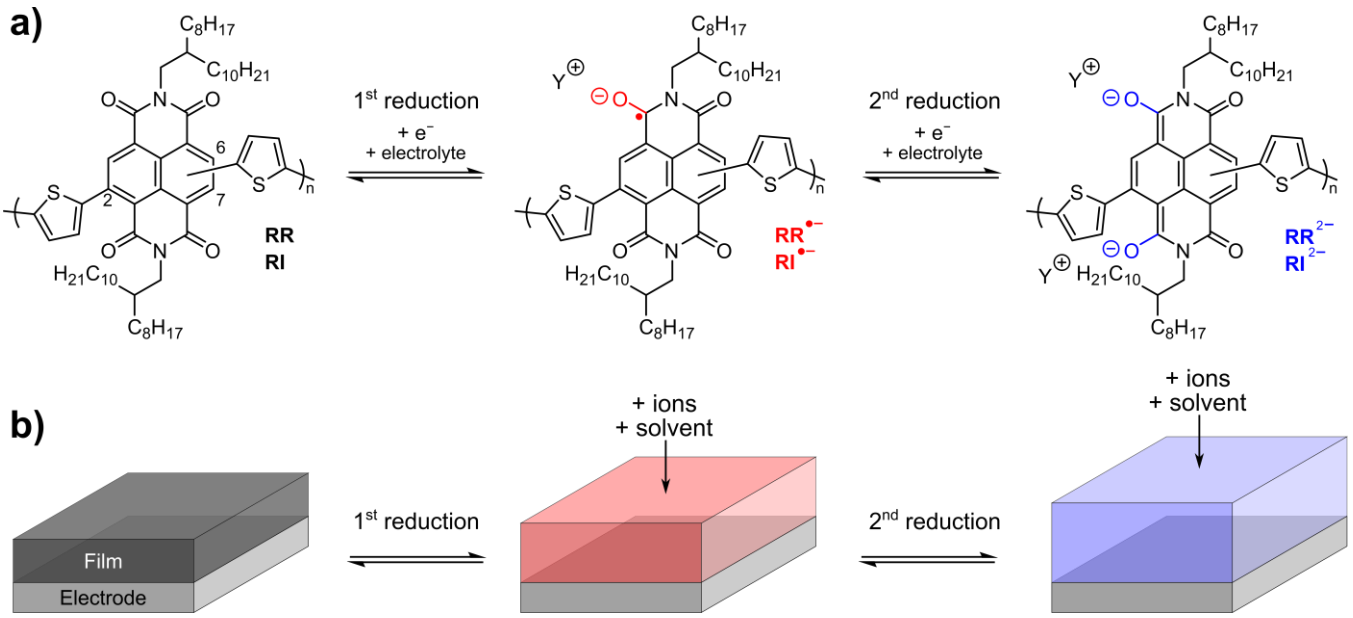

Scheme 1. a) Chemical structure of RR- and RI-P(NDI2OD-T_2) and corresponding species occurring upon electrochemical reduction or chemical doping. RR: purely 2,6-linked monomer units; RI(70:30): 70 % 2,6- linkage and 30 % 2,7-linkage; RI(47:53): 47 % 2,6- linkage and 53 % 2,7-linkage; RI(24:76): 24 % 2,6- linkage and 76 % 2,7-linkage. b) Simplified sketch of the two-fold electrochemical reduction accompanied by electrolyte entrance for maintaining electroneutrality.

In a first step, we looked into the electrochemical doping behaviour, i.e. reduction behaviour of P(NDI2OD-T_2) (see Scheme 1). The regioregular system RR with solely 2,6-linked monomer units is compared with the regioirregular counterparts RI(70:30), RI(47:53) and RI(24:76). The synthesis is described elsewhere, polymer characteristics are given in the experimental section.[17]

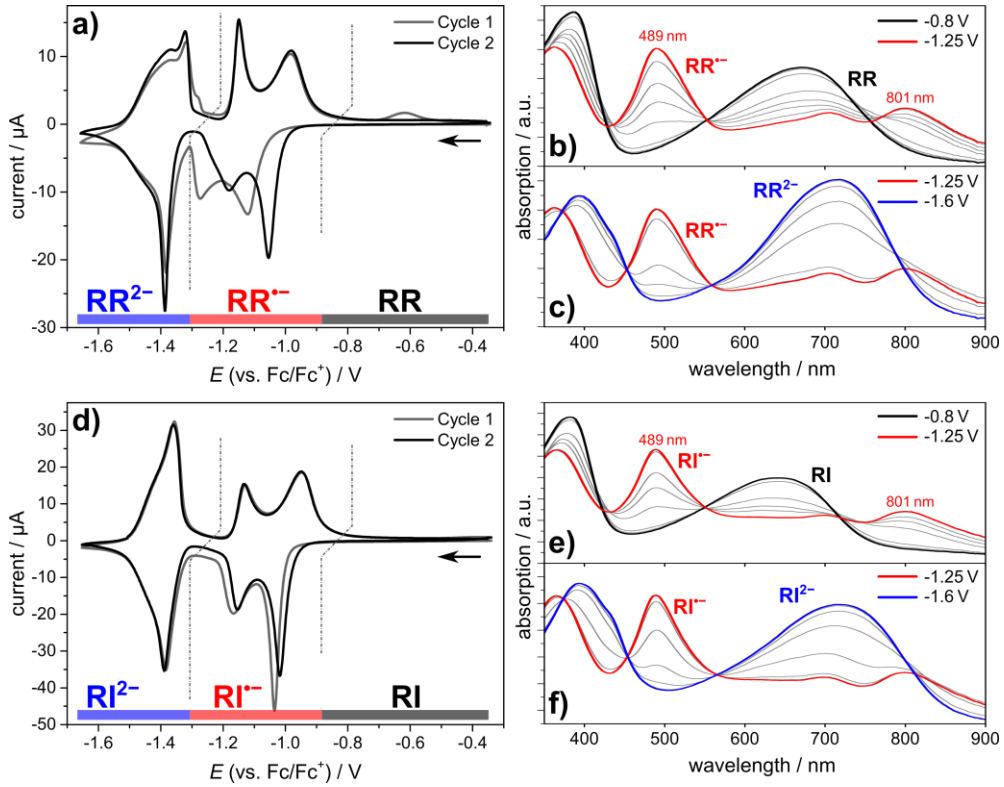

Figure 1. Electrochemical characteristics of RR (a-c) and RI(47:53) (d-f). Cyclic voltammograms (a, d) of films spin-coated from $CHCl_3$ on ITO as working electrode in 0.1 M NBu_4PF_6/MeCN as electrolyte, scan rate 20 mV/s. UV-Vis spectra of RR (b,c) and RI(47:53) (e,f) recorded during the forward scan in the 2nd cycle, the spectra are divided into the first (−0.8 to −1.25 V) and second (−1.25 to −1.6 V) reduction.

Figure 1 a) shows the first (grey) and second cycle (black) of a cyclic voltammogram of the RR polymer film. The data discussion will be started with the 2nd cycle. During reduction of the polymer two sets of signals between -0.9 to -1.25 V (red) and -1.3 to -1.6 V (blue) become apparent. Both sets consist of several overlapping reduction and reoxidation waves and are reversible for all further cycles. Half wave potentials of the three main signals are $E^{Ia}_{1/2}$ = -1.02 V, $E^{Ib}_{1/2}$ = -1.17 V and $E^{II}_{1/2}$ = -1.36 V, respectively. From the first reduction a lowest unoccupied molecular orbital (LUMO) level of -4.08 eV can be estimated, assuming a formal potential of -5.1 eV for the ferrocene/ferrocenium redox couple (Fc/Fc^+) in the Fermi scale.[39] During reduction, solvated electrolyte ions diffuse into the polymer film for charge neutralization which is often accompanied with swelling of the film.[40]

Figure 1 b) and c) show the corresponding UV-Vis spectra measured during the 2nd forward cycle from -0.8 V to -1.25 V and -1.25 V to -1.6 V, respectively. From -0.4 to -0.8 V the

neutral polymer absorption is observed, with two maxima at 385 and 671 nm, which are ascribed to a π−π* transition and the intramolecular charge-transfer band, respectively.[11,41] Upon reduction a gradual decrease in the neutral absorption bands occurs and new absorption bands with maxima at 362, 489, 708 and 801 nm arise which can be assigned to the radical-anion $RR^{\bullet-}$ species. The appearance of the new species is also evidenced by three isosbestic points in the spectra. In particular, the bands at 489 and 801 nm continue to grow at wavelengths where the neutral absorption does not superimpose the radical-anion absorption. Below a potential of -1.25 V the radical-anion band decreases again and new absorption maxima at 392 and 717 nm grow. Again, three isosbestic points can be identified, suggesting the reduction to the RR^{2-} dianion.

Reducing films of the regioirregular polymers gives similar courses of the cyclic voltammogram in the 2nd cycle (Figure 1 d) and Figure S 1). The CV of RI(47:53) (black, Figure 1, d) gives half-wave potentials of $E^{Ia}_{1/2}$ = -0.99 V, $E^{Ib}_{1/2}$ = -1.14 V and $E^{II}_{1/2}$ = -1.35 V with a LUMO value at -4.11 eV which is similar to RR. The spectral change while reducing RI to $RI^{\bullet-}$ and from $RI^{\bullet-}$ to RI^{2-} is shown in Figure 1 e) and f), respectively. The neutral RI shows maxima at 382 and 643 nm, which corresponds to a blue shift of the charge-transfer band of around 30 nm compared to RR. This can be attributed to the reduced aggregation tendency in regioirregular polymers due to the disruption of the polymer chain by the regioirregular linkage.[17] The decrease of the neutral band clearly matches with the onset of reduction to the radical-anion $RI^{\bullet-}$ in the CV. Interestingly, the absorption maxima at 362, 489, 701 and 801 nm of the reduced $RI^{\bullet-}$ are very similar to the $RR^{\bullet-}$ bands and differ less than in the neutral state of both polymers. At potentials below -1.3 V the polymer is further reduced and RI^{2-} bands occur at 392 and 714 nm.

First Cycles

The attention is now turned to the comparison of the first and second cycles of the RR and RI films. The very first cycle of RR (Figure 1 a), grey) features signals shifted to lower potentials and differs especially in the first reduction set to that of the second cycle. Two main reduction waves with peak potentials of -1.12 V and -1.27 V are observed, which is in accordance to our earlier studies.[27] One possible reason for the first cycle effect is the high order and dense packing in the RR films. It has to be kept in mind that electrochemical doping always involves counterion and solvent diffusion into the films to ensure electroneutrality which is accompanied by swelling of the films. Denser films can lead to hindered diffusion of counter ions and solvent into the film upon reduction.[40] This behavior is morphology dependent and even more pronounced in more ordered films obtained by annealing at 220 and 300 °C, respectively.[27] For the RI systems on the other hand the 1st cycle (Figure 1, d), grey for RI(47:53)) shows no pronounced shift of the potentials and is almost overlapping with the 2nd cycle. From these data a facilitated diffusion of counter ions and solvent into the film upon reduction might be proposed. This would be consistent with the more amorphous and less aggregated nature of the regioirregular films.[17,27]

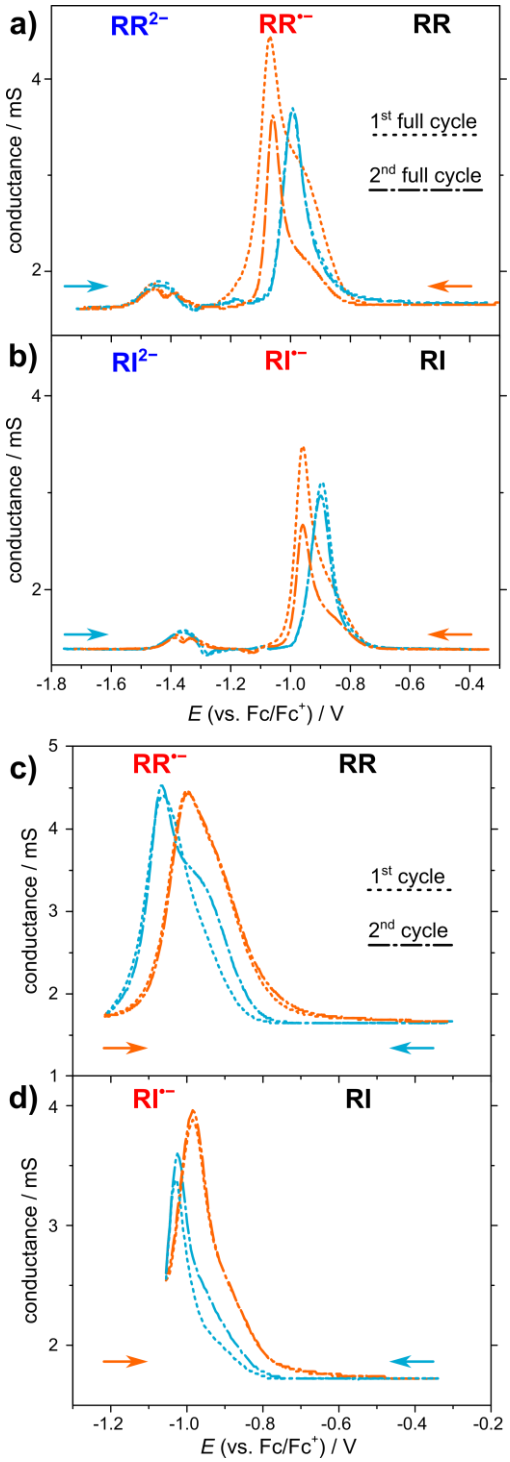

Figure 2. In-situ conductance (1st and 2nd full cycles) of RR (a) and RI(47:53) (b) films spin coated from $CHCl_3$ (c = 3 g/l) on interdigitated Pt electrodes. Blue is the forward and orange the backward scan. In-situ conductance (1st and 2nd cycle) of RR (c) and RI(47:53) (d) films spin coated from $CHCl_3$ (c = 3 g/l) on interdigitated Pt electrodes at a lower vertex potential around -1.1 V. The potential difference between the two interdigitated combs is 10 mV. The measurements were performed in NBu_4PF_6/MeCN as electrolyte with a scan rate of 10 mV/s.

To shed light on the conducting state in such polymers, the conductance as function of applied potential was measured with an organic electrochemical transistor configuration, Figure 2 a) and b).[42] The cyclic voltammograms on the Pt electrodes are identical to those discussed above, the forward scans are drawn in blue and the backward scan in orange. The conductance profile in the first full cycle shows two maxima, one at potentials corresponding to the first reduction to $RR^{\bullet-}$ around -1.0 V and one during the second reduction to the dianion RR^{2-} around -1.45 V. Interestingly, the maximum conductance at the radical-anion state $RR^{\bullet-}$ is higher compared to the dianion state RR^{2-}. Furthermore, a decrease of the overall conductance is observed in the backward scan and remains at these low values in all further cycles. In the second full cycle the conductance profile is reversible both in the forward and in the backward scan.

The formation of maxima instead of a conductance plateau, as e.g. observed for polythiophenes, indicates a different charge transport mechanism compared to classical conjugated polymers.[40,43,44] This can be mainly attributed to localized charges on the naphthalenediimide units which involves a hopping mechanism between different redox sites rather than delocalization along the polymer backbone.[45,46] This mixed-valence conductivity is observed also for redox-polymers, which associates RR to the class of conjugated redox-polymers.[27,31] Both temperature dependent measurements of charge carrier mobility in organic field effect transistors and results from charge modulation spectroscopy support these findings.[47,48] The drop of the maximum of the in-situ conductance from the forward to the backward scan of RR is presumably due to a kind of overdoping or to an excessive degree of swelling and change of the film morphology through the formation of flow channels, thus diminishing charge transport.

To address these issues, the in-situ conductance was investigated at different vertex potentials (see also Supporting Information). Figure 2 c) shows the in-situ conductance of RR in the potential regime of –0.35 to –1.1 V (vs. Fc/Fc) where the radical-anion is observed in the

corresponding in-situ spectroelectrochemistry data. In these data the conductance does not drop and remains stable over numerous cycles. This is a strong indication that the second reduction does cause the decrease in conductance. This process might be the incorporation of even more counter ions – in addition to the incorporation during the first reduction – and further swelling of the film, which is a plausible reason why the in-situ conductance irreversibly decreases upon cycling to very low potentials.

The in-situ conductance profile of RI(47:53) is shown in Figure 2 b). The profile of the first full cycle shows two maxima at a potential around -0.95 V ($RI^{\bullet-}$) and of -1.38 V (RI^{2-}), respectively, which are shifted to slightly higher potentials compared to RR. Again, a profile with two maxima is observed, however, differences between the forward and backward cycle are less pronounced, concurrent with the observations in the CVs. Although RI(47:53) seems to have a less ordered structure and should therefore allow easier intercalation of countercations upon reduction, reduction to the dianion decreases the maximum conductance as well. Electrochemical measurements of the two regioirregular polymers RI(70:30) and RI(24:76) are in line with the results for RI(47:53), Figure S 1. Irrespective of the chemical linkage found in the regioirregular polymers, the redox units are the same, explaining a related charge transport by hopping processes in RI, also leading to similar conductance profiles. Overall the regioirregular systems seem to enable a facilitated diffusion of counterions and solvent into the films which can be seen by lower differences in the first and second cycles. This is reasonable and can be explained by less order in the films due to a lower degree of aggregation.

Different countercations were used to see if the ion size has an impact on the conductivity, however, the decrease in conductance is observed for both RR and RI(47:53) in NMe_4PF_6, NBu_4PF_6 and $NHex_4PF_6$, as shown in Figure S 3.

From these experiments important insights in the reduction / doping behaviour of RR and RI P(NDI2OD-T2) are obtained. 1) In-situ spectroelectrochemistry allows the identification of two charged states (radical-anion and dianion) upon reduction which are not sensitive to regioisomerism. 2) Organic electrochemical transistor measurements suggest mixed valence conductivity of P(NDI2OD-T_2) with a maximum conductance observed in the radical-anion state. 3) For all systems conductivity is reduced when charging is performed until the dianion state and fully reversible when staying in the potential window for the radical-anion. 4) For all regioirregular systems no first cycle effect in the cyclic voltammograms are observed which can be explained by a more isotopic and easier accessible structure for reversible charging.

Chemical Doping of Regioirregular Films.

Encouraged by the in-situ conductance measurements, the conductivity was tested with external chemical doping strategies. As mentioned in the introduction the search for chemical dopants of P(NDI2OD-T_2) is not straightforward. To allow comparison with literature data, N-DMBI was used for solution doping and TDAE for vapor doping in the following study (for chemical structures see Figure 3 a). Since miscibility problems and thus ineffective doping were already described in literature,[28] advantage was taken of tunable aggregation in the regioirregular polymers by different amounts of 2,6- and 2,7 linkage of the repeating units. For organic solar cells it had been shown that a lower degree of aggregation can indeed lead to a better mixing in the blends, resulting in superior performance when regioirregular P(NDI2OD-T_2) was used as acceptor.[17] Also from the electrochemical investigations on regioirregular systems a less ordered film structure and better diffusion of counter ions is apparent, which might facilitate polymer/dopant miscibility. Less order and interaction between several polymer chains could potentially also enable a better diffusion/penetration of the TDAE dopant vapor into the polymer film.

Solution Doping with N-DMBI

The typical procedure for doping with N-DMBI in the literature includes mixing of the polymer with the dopant at room temperature (I), solution-deposition of the blends into films (II) and inducing the doping reaction upon heating (III).[28] The optimized procedure for the experiments in the following is mixing of stock solutions, spin coating, followed by heating of the blend films for 3 h at 55 °C in an inert atmosphere (see also Figure S 4). To study the reaction success, UV-Vis absorption spectra were recorded after heating in inert conditions.

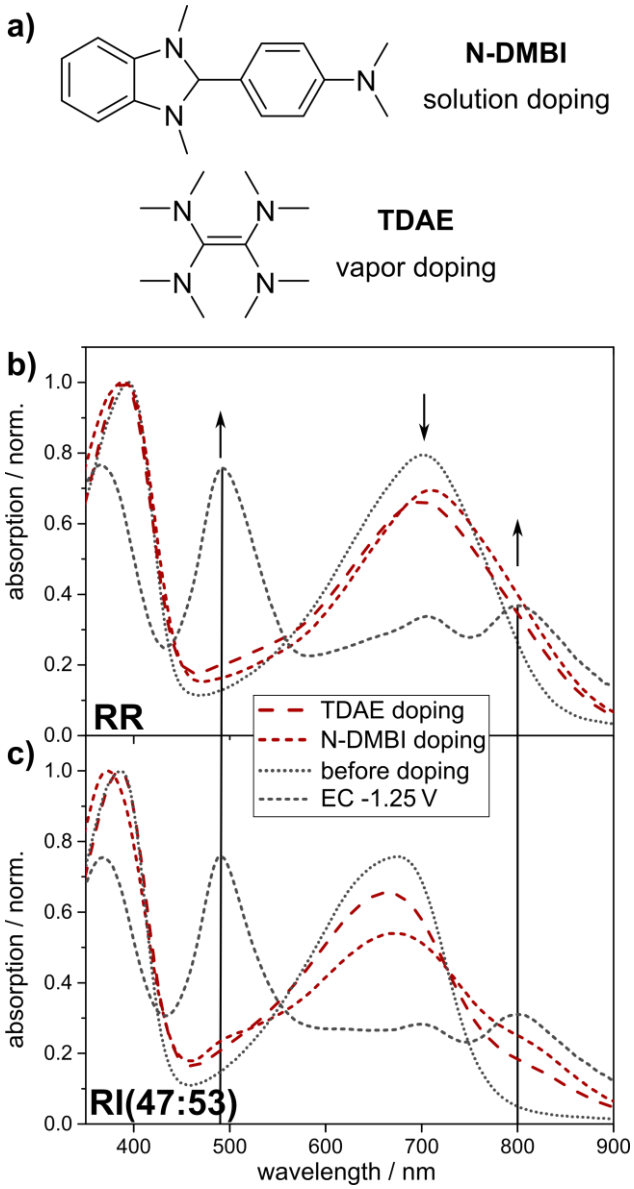

Figure 3. a) Chemical structures of N-DMBI and TDAE. UV-Vis spectra of spin-coated films of RR (b) and RI(47:53) (c) before doping (grey dotted lines) and upon solution doping with N-DMBI (50 mol%, red dotted lines) and vapor doping with TDAE (35 °C, 2 h, red dashed lines). Radical-anion bands at 489 and 800 nm are highlighted and for comparison spectra taken at –1.25 V are shown (from Figure 1, grey dashed lines).

Compared to the absorption of the neutral RR film, the absorption profile of a 50 mol% N-DMBI doped RR film (Figure 3 b) shows a rather weak absorption increase at 489 nm and 800 nm and only little changes of the neutral band at 710 nm. These data suggest that doping to the radical-anion state is happening, but only to a small extent compared to the in-situ spectroelectrochemistry results. Doping of the regioirregular films shows similar trends, as displayed in Figure 3 c) and Figure S 5. The only difference is that slightly more distinct radi-

cal-anion bands at 489 and 800 nm are visible. With increasing 2,7-linkage in the regioirregular polymers the charge-transfer band of the neutral polymer gets less pronounced and blue shifted,[17] leading to the stronger visibility of the second maximum of the radical-anion around 800 nm in doped films.

Table 1. Conductivity values for N-DMBI and TDAE doping of RR, RI(70:30), RI(47:53) and RI(24:76).

	RR	RI(70:30)	RI(47:53)	RI(24:76)
	Conductivity σ / S/cm			
25 mol% N-DMBI	$(5.7 \pm 1.1) \times 10^{-4}$	$(4.6 \pm 0.7) \times 10^{-4}$	n .d.	n .d.
50 mol% N-DMBI	$(1.6 \pm 0.2) \times 10^{-3}$	$(2.2 \pm 0.2) \times 10^{-3}$	$(6.1 \pm 0.6) \times 10^{-4}$	$(4.5 \pm 0.6) \times 10^{-4}$
TDAE	$(2.3 \pm 0.3) \times 10^{-3}$	$(7.5 \pm 0.7) \times 10^{-4}$	$(3.9 \pm 1.3) \times 10^{-4}$	$(4.4 \pm 0.4) \times 10^{-4}$

Conductivity values of films doped with 25 and 50mol% N-DMBI are listed in Table 1. The measurements were performed with a 4-line-probe method where four terminal sensing eliminates contact resistances occurring at the probe/electrode or electrode/film interface.[49] The conductivities are $\sigma = 5.7 \cdot 10^{-4}$ S cm^{-1} for 25 and $\sigma = 1.6 \cdot 10^{-3}$ S cm^{-1} for 50 mol% doped RR films. Additionally, RI(70:30), RI(47:53) and RI(24:76) were doped with N-DMBI and the conductivity was measured to clarify the influence of regioregularity. Although featuring a lower charge carrier mobility,[17] spin coated RI(70:30) can be doped with 25 and 50 mol% N-DMBI to conductivities of $\sigma = 4.6 \cdot 10^{-4}$ and $\sigma = 2.2 \cdot 10^{-3}$ S cm^{-1}, which is as high as for RR. For RI(47:53) and RI(24:76) doped with 50 mol% N-DMBI, slightly lower values around $5 \cdot 10^{-4}$ S cm^{-1} are found. Higher dopant amounts of 100 mol% N-DMBI lead to a slight decrease in conductivity (RR: $\sigma = 1 \cdot 10^{-3}$, RI(70:30): $\sigma = 7 \cdot 10^{-4}$ S cm^{-1}).

AFM images (Figure S 6) of all polymers doped with N-DMBI show clustering of the dopant on the top surface. This implies a rather poor miscibility of polymer and dopant molecules, fitting to observations in similar systems in literature.[28,31] Also the blends with the regioirregular polymers do not seem to improve the mixing with the dopant.

Vapor Doping with TDAE

Next, we used the electron rich vapor dopant TDAE which is known to be a reducing agent for fullerenes and polymers.[50,51] TDAE has a reduction potential of -1.08 V vs. Fc/Fc^+ which is in the potential range of the first reduction of P(NDI2OD-T_2) (Figure 1).[39,52] The advantage of vapor doping is that it is a post-deposition technique and the film morphology can be precisely controlled before the actual doping procedure is started. No dopant molecules can disturb the film formation process which should lead to higher order in the thin films.

After optimizing the vapor doping time and temperature procedure (see supporting information), spin coated films were doped in TDAE vapor at 35 °C for 2 h and first their UV-Vis absorption behavior was investigated. The absorption spectra are shown in Figure 3 b) and c) for RR and RI(47:53), respectively. Similarly to what is observed with N-DMBI, the overall absorption of the radical-anion is hardly visible at 489 and 800 nm for the RR system and is slightly more pronounced for the regioirregular systems (Figure S 7 for RI(70:30) and RI(24:76)).

RR films show conductivities of $\sigma = 2.3 \cdot 10^{-3}$ S cm^{-1} after doping in TDAE vapor, which is comparable to 50 mol% N-DMBI doped films. Less aggregated systems as found in the regioirregular polymers show conductivities of $\sigma = 7.5 \cdot 10^{-4}$, $\sigma = 3.9 \cdot 10^{-4}$ and $\sigma = 4.4 \cdot 10^{-4}$ S cm^{-1} for RI(70:30), RI(47:53) and RI(24:76), respectively. The values are summarized in Table 1. AFM images (Figure S 8) of the polymer films show a rather homogeneous surface and no clusters were observed. This is in contrast to films doped with N-DMBI. While for doping of RI(70:30) with N-DMBI similar conductivities to those of RR were found, the conductivities measured with TDAE remain slightly lower for the regioirregular polymers.

Discussion of N-DMBI and TDAE Doping of RR and RI Films.

When RR films were doped, both dopants showed conductivities around $\sigma = 2 \cdot 10^{-3}\,S\,cm^{-1}$, which are in the same order of magnitude as for comparable systems in literature ($1-8 \cdot 10^{-3}\,S\,cm^{-1}$).[28,31,38,53] With N-DMBI a maximum conductivity could be observed at 50 mol% of dopant. One main reason for this observation might be the strong clustering of dopant molecules which was observed for all dopant concentrations in atomic force microscopy. Consequently, only a very low doping efficiency is present, which was quantified in literature to only 1 %.[28,31] A small extent of doping is supported by the UV-Vis absorption after doping. Similarly, Wang et al. observed high conductivities at rather low radical-anion absorption,[54] and no clear correlation with the UV-Vis absorption could be found for both N-DMBI and TDAE doping. The low efficiency is presumably the reason for various different polymer/N-DMBI ratios given in different manuscripts in literature for achieving the highest conductivity. Furthermore, this might be the reason that processing conditions are dissimilar in different investigations of independent research groups. No pure redox reaction but a hydride transfer is proposed as doping mechanism for P(NDI2OD-T2)/N-DMBI doping, which complicates comparison between electrochemical and chemical doping behavior with N-DMBI even further.

Despite these issues, the regioirregular polymers RI(70:30), RI(47:53) and RI(24:76) could be successfully doped with N-DMBI and TDAE and similar conductivities of RI(70:30) compared to RR were measured. Lower values for RI(47:53) and RI(24:76) might be explained by even lower order in the films and thus hindered charge transport or an altered diffusion of the TDAE dopant vapor into the films.

These findings suggest that independent of mobility, the conductivity seems to saturate in this polymer at around $2 \cdot 10^{-3}\,S\,cm^{-1}$. Naab et al. could show that the proportionality between mobility and conductivity is not always given in this and similar naphthalenediimide and perylenediimide polymers.[38] It was proposed that the strong donor-acceptor character of

P(NDI2OD-T_2) leads to a strong localization of the charges on the backbone and thus rather localized polarons with inefficient charge transport. More planarized NDI-based polymers with reduced donor–acceptor character were recently demonstrated to achieve higher conductivities.[55] On the other hand, neither N-DMBI nor TDAE reveal a strong radical-anion absorption after doping. It remains unclear if more charges in the backbone might also exceed the conductivity values of 10^{-3} S cm^{-1}. In the following we use highly defined polymer morphologies to further understand the chemical doping behavior.

Structural Analysis of Chemically Doped Anisotropic Films.

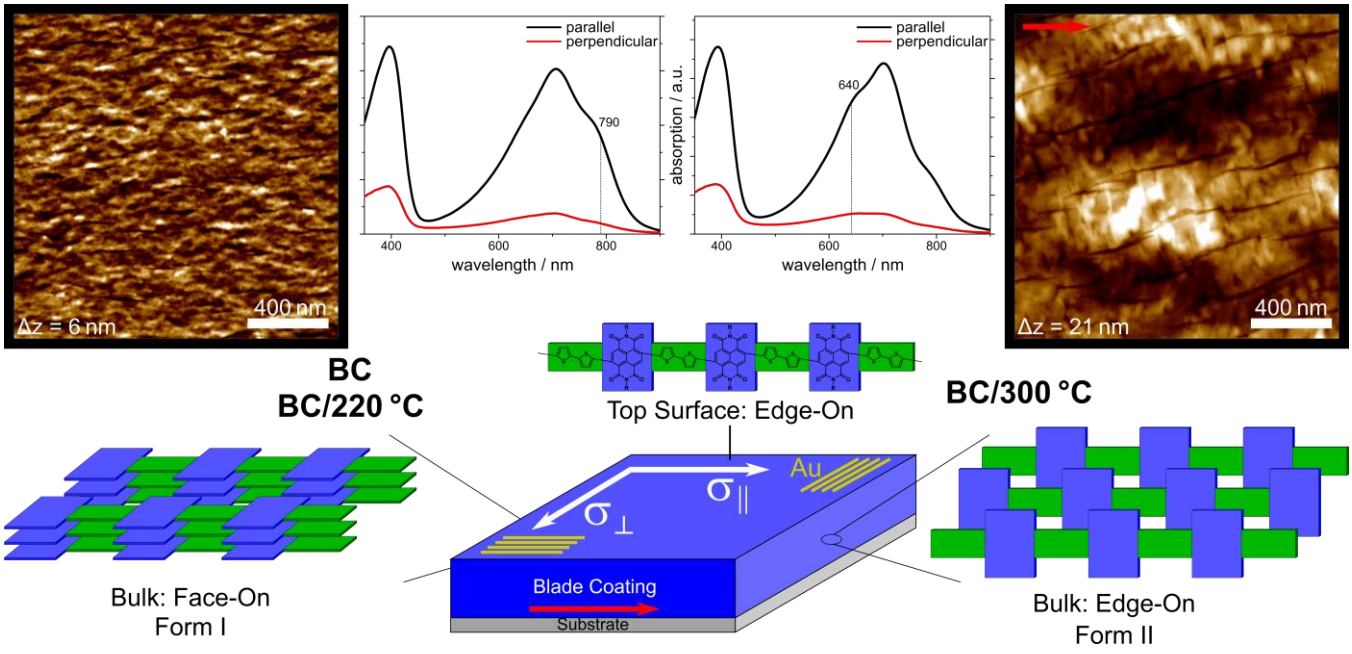

Figure 4. Blade coating of aggregated polymer solutions to prepare anisotropic films. A fibrillar structure is observed in AFM of BC and BC/220 °C films, ribbons are present in AFM micrographs of BC/300 °C films. Anisotropy is probed by polarized UV-Vis spectroscopy parallel and perpendicular to the blade coating direction. Electrodes for four line probe conductivity measurements are shown schematically on a blade coated film. Conductivities are measured parallel ($\sigma_{||}$) and perpendicular ($\sigma_{\perp}$) to the blade coating/chain direction. Schematic representations of the thin film morphologies after BC and BC/220 °C (face-on, form I) and BC/300 °C (edge-on, form II). Irrespective of the bulk morphology, at the top surface an edge-on orientation of the polymer chains is observed.

While the direction dependence of absorption and charge carrier mobility has been well addressed for P(NDI2OD-T_2), no reports in literature focus on the anisotropy in conductivity. Here, we follow a blade coating (BC) protocol which has been recently reported as a versatile and easy method to prepare anisotropic P(NDI2OD-T_2) films from aggregated chlorobenzene solutions.[15] To summarize the procedure and the resulting morphologies: Preparation of aligned homogeneous P(NDI2OD-T_2) films with thicknesses between 30-40 nm can be achieved by blade coating of polymer solutions in chlorobenzene. Three different sample preparations will be compared: (I) as-cast blade coated films (BC), (II) blade coated films annealed at 220°C (BC/220°C) and (III) blade coated films annealed at 300°C (BC/300°C). The BC and BC/BC220°C films show a face-on morphology in bulk with polymorph form I (segregated stacking) and the BC/300°C films (mixed stacking) yield an edge-

on morphology in bulk with polymorph form II.[15,20,56] All films have an edge-on oriented layer on the top surface. Dichroic ratios ($DR = A_{\parallel} / A_{\perp}$) determined by polarized UV-Vis spectroscopy parallel and perpendicular to the blade coating direction of the films gave values of 8 and above. The polymorphism is evidenced by ED, but can be also seen in the absorption spectra: a 790 nm absorption shoulder is characteristic for Form I and a 640 nm absorption shoulder for Form II. For the in-depth structural characterization we refer to reference 15.

The oriented P(NDIT2OD-T2) films were doped either with N-DMBI or with TDAE to make them conductive. As a matter of facts, N-DMBI doping was difficult since bladecoating and N-DMBI doping interfere (see experiments and discussion in the supporting information). Therefore, we will essentially focus in the following on the TDAE-doping from the vapor phase that allows to investigate the impact of initial film structure and morphology on the resulting electronic properties of the TDAE-doped films. Dichroic ratios were determined by polarized UV-Vis measurements and before doping values of DR = 7.9, 8.0 and 8.4 were found for BC, BC/220 °C and BC/300 °C films, respectively. Vapor doping was performed at 35 °C for 2 h in a sealed Petri dish. Alignment of the polymer chains seemed not to suffer from the doping process, as the polarized absorption after TDAE doping parallel is still significantly higher compared to perpendicular to the BC direction (Figure S 13). As discussed above due to the spectral change in the absorption spectrum upon generation of radical-anions, no dichroic ratios were calculated. Atomic force micrographs indicate that alignment is maintained after doping, even though clusters of dopant seem to be present on the film surface (Figure S 14).

The conductivities of the BC film parallel and perpendicular to the blade coating direction are $\sigma_{\parallel} = 3.3 \cdot 10^{-3}$ and $\sigma_{\perp} = 1.2 \cdot 10^{-3}$ S cm^{-1}, respectively, corresponding to an anisotropy in conductivity of 2.8. Isotropic films by spin coating have conductivities of $\sigma = 2.3 \cdot 10^{-3}$ S cm^{-1}, which is in between the values of parallel and perpendicular obtained by blade coating. BC/220 °C films show conductivities of $\sigma_{\parallel} = 7.7 \cdot 10^{-3}$ and $\sigma_{\perp} = 1.3 \cdot 10^{-3}$ S cm^{-1} and maximum

values reach $\sigma_{||} = 8.3 \cdot 10^{-3}$ S cm^{-1}. An anisotropy factor of 5.9 is reached, which is the highest value reported for conductivities for P(NDI2OD-T_2) so far. BC/300 °C films show slightly lower values of $\sigma_{||} = 1.8 \cdot 10^{-3}$ and $\sigma_{\perp} = 4.5 \cdot 10^{-4}$ S cm^{-1}, with an anisotropy of 4.0. The values are summarized in **Erreur ! Source du renvoi introuvable.**.

Table 2. Conductivity values and anisotropy factors after TDAE doping in anisotropic blade coated films.

	Doping with TDAE		
	BC	**BC/220 °C**	**BC/300 °C**
$\sigma_{\|}$ / S·cm^{-1}	(3.3 ± 1.6) × 10^{-3}	(7.7 ± 0.6) × 10^{-3}	(1.8 ± 1.4) × 10^{-3}
$\sigma_{\perp}$ / S·cm^{-1}	(1.2 ± 0.2) × 10^{-3}	(1.3 ± 0.2) × 10^{-3}	(4.5 ± 1.8) × 10^{-4}
$\sigma_{\|}$ / $\sigma_{\perp}$	2.8	5.9	4.0

Transmission electron microscopy was used to gain a more detailed understanding of the doping process in the polymer films. Films were blade coated on glass substrates, removed from the substrate by floating on dilute HF solution and recovered on TEM grids. The films were then annealed to 220 °C or 300 °C to yield the target morphologies/polymorphs and subsequently doped with TDAE vapor. Figure 5 shows the ED patterns of both a) BC/220 °C and b) BC/300 °C films with and without TDAE doping, respectively. Additionally, cross-section profiles of the ED patterns along the meridian and equator are shown. The d_{hkl} values evaluated from the reflections are summarized in Table 3.

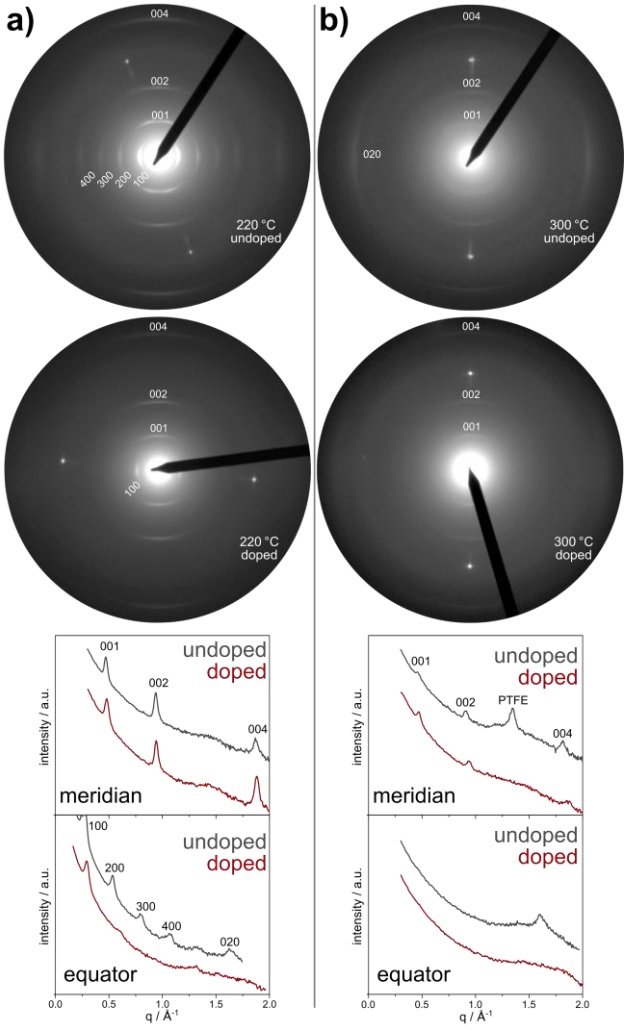

Figure 5. Comparison of the TEM-ED diffraction patterns of doped and undoped P(NDI2OD-T_2) blade-coated films. a) The left patterns correspond to BC/220 °C and b) the right images to BC/300 °C films. Cross-section profiles along the meridian and equator show the relative intensities of the diffraction peaks along the alkyl (*h*00), π-stacking (0*k*0) and backbone (00*l*) directions.

Table 3. Calculated distances from TEM-ED reflections in BC/220 °C and BC/300 °C before and after doping with TDAE vapor at 35 °C for 2h. Accurate diffraction distances were obtained by calibration with an oriented PTFE film on a second TEM copper grid, which was put on top of the doped film. The 100 PTFE reflection observed corresponds to a distance of 4.9 Å.[56,57]

	d_{hkl} / Å						
	001	**002**	**004**	**100**	**200**	**300**	**020**
BC/220 °C	13.9	7.17	3.58	25.1	12.5	8.36	-
BC/220 °C doped	13.6	6.85	3.42	21.6	-	-	-
BC/300 °C	14.2	7.27	3.65	-	-	-	4.10
BC/300 °C doped	13.4	6.75	3.39	-	-	-	-

BC/220 °C Samples

BC/220 °C films show the typical reflections present in face-on oriented polymer chains with polymorph form I. This was assigned according to previous studies on P(NDI2OD-T_2) with directional epitaxial crystallization on 1,3,5-trichlorobenzene and high-temperature rubbing and subsequent annealing below 280 °C.[20,56] Recently, we showed that blade coating and annealing at 220 °C also leads to the observed morphology, albeit for polymers of lower molecular weight (Mn=XXX).[15] The presence of a faint 020 reflection could result from edge-on oriented chains on the film surface, which was also observed by near-edge X-ray absorption fine structure (NEXAFS) spectroscopy.[15] The observation of (*h*00) reflections up to the fourth order in the alkyl direction and rather narrow diffraction arcs support the high alignment in the films, as it was also observed by polarized UV-Vis spectroscopy.

TDAE doped samples display a less-defined ED pattern compared to BC/220 °C. Most prominent on the first view is the loss of higher order (*h*00) reflections along the side chain direction: only the 100 reflection remains visible after doping. This indicates a lower degree of order along this crystallographic direction, which could be explained by the intercalation of the dopant molecules between the alkyl chains. Hence, the distance between the chains should increase, as an additional molecule between the chains needs a certain amount of space. Surprisingly, the d_{100} value calculated from the observed reflection is 21.6 Å, which is 3.5 Å shorter than for the undoped sample. The decrease in the d_{100} alkyl spacing is concurrent with a decrease of the backbone periodicity from d_{001}=13.9 to 13.6 Å (higher-order reflections 002 and 004 correspond to 6.85 Å and 3.42 Å periodicities). GIWAXS measurements on TDAE doped P(NDI2OD-T_2) in literature showed also a reduction in the lamellar reflexes (in-plane) and a smoothing of the out-of-plane π-stacking peak.[54]

Simultaneous decrease of both alkyl and backbone distance could have several origins. In form I, the a and c axes (along the side chains and backbone, respectively) make an angle β= 76°.[20,56] A simultaneous reduction of the d_{100} and d_{001} reticular distances could in principle

reflect a change in the β angle. However, this would imply the 001 reflections to depart from the meridional position which is contrary to the observation of a meridional 001 after doping. In other words, the original monoclinicity of the P(NDI2OD-T_2) form I unit cell is lost after doping with TDAE whereas it should be enhanced in the case β decreases. Therefore, a change in the β angle seems not likely to explain the changes of the ED pattern upon doping.

As an alternative explanation, the reduction of the d_{001} periodicity can also be due to a change in the P(NDI2OD-T_2) backbone conformation. NEXAFS studies and vibrational spectroscopy showed that a dihedral angle θ around 40° between the naphthalenediimide and bithiophene units is present, even if on average the P(NDI2OD-T_2) chains lie preferentially face-on with respect to the substrate.[58–61] Additionally, a torsional angle τ around 148° exists between the two thiophenes (see also Figure S 15).[60,62] Depending on the dihedral angles θ and τ, and the value of β, different d_{001} periodicities along the polymer backbone can be obtained. Also computational results on charged species showed changes in the bond lengths and torsional angles upon oxidation or reduction.[63] Accordingly, TEM ED evidences a sizable change in the unit cell parameters of form I after TDAE doping possibly related to a change of backbone conformation.

BC/300°C Samples

In non-doped BC/300 °C samples, a preferential edge-on orientation of the P(NDI2OD-T_2) with polymorph form II (mixed stacking) is observed both in literature and in the work presented here.[15,20,56] This can be seen from reflections along the meridian assigned to the backbone (00*l*) and the π-stacking reflection 020 with a distance of 4.1 Å. The ED pattern confirms polymorph form II in BC/300 °C films, given the dominant intensity of the 002 reflection over the 001.

After doping with TDAE vapor for 2 h, no π-stacking reflection can be observed anymore, which indicates an important reduction in the ordered packing of P(NDI2OD-T_2)

chains. This is in line with recent results by Wang et al., who observed a disruption of the π-stacking of TDAE doped P(NDI2OD-T_2) films by GIWAXS measurements.[55] Due to missing π-stacking or lamellar reflections, no assignment of face-on or edge-on is possible in BC/300 °C doped samples. Similar to the BC/200 °C samples, a reduction of the periodicity along the backbone is observed (the d_{00l} distances are 13.4, 6.75 and 3.39 Å for l=1,2 and 4, respectively). The cross-sectional profiles along the meridian demonstrate an increase in scattering intensity of the 001 reflection. This is the fingerprint of polymorph form I and reveals a shift of the polymer chains along the *c*-direction from a mixed stacking in the undoped films to a segregated stacking after doping. The polarized UV-Vis absorption of a less doped BC/300 °C film in Figure S 16 supports this finding, as no absorption shoulder around 640 nm is present after doping.[20,56] In the thermodynamically stable form II, electron rich T_2 and electron poor NDI2OD are stacked on top of each other. If the electron rich dopant TDAE dopes the polymer and incorporates between the chains in the π-stacking plane, an additional electron rich molecule is present in the polymer film. TDAE molecules could thus disrupt the original mixed stacking (form II) of T_2 and NDI2OD. This could further explain the transformation of form II back to form I after doping.

No crystallites of the dopant molecules are observed in both BC/220 °C and BC/300 °C samples, thus no larger domains of the dopants seem to be present in the film. Additionally, the change of the TEM-ED patterns evidence doping of the bulk. At no point two crystalline phases, i.e. doped and undoped are observed, which indicates a uniform doping of all crystalline domains in the film. This is an important finding, which is not given by AFM or UV-Vis measurements. No significant broadening of the diffraction arcs can be observed, suggesting that the alignment of the polymer chains is preserved. This is in line with polarized UV-Vis spectra having qualitatively similar dichroic ratios before and after doping.

Discussion of TDAE Doped Anisotropic Films.

All films indeed show an anisotropic charge transport in conductivity of 2.8, 5.9 and 4.0 for BC, BC/220 °C and BC/300 °C films, respectively. However, as the dichroic ratio measured by polarized UV-Vis was around 8 for all samples, this is unexpectedly low. Lower anisotropies in conductivity compared to electron mobility could indicate an inherently less dependent transport on chain alignment in P(NDI2OD-T_2). The charge carrier channel in transistors is at the interface between dielectric layer and polymer, while in conductivity measurements charge carriers move three-dimensionally through the bulk. This is a fundamental difference and could explain different anisotropies and might even prevent the comparison of mobility and conductivity anisotropies. Likewise, for P3HT a dichroic ratio of 50 was obtained after high-temperature rubbing, while a conductivity anisotropy of 8–10 was found in F_4TCNQ doped samples.[24] The maximum conductivity of $\sigma_{||} = 8.3 \cdot 10^{-3}\,\mathrm{S\,cm^{-1}}$ parallel to the chain is among the highest conductivities for P(NDI2OD-T_2) and even slightly higher measured here with TDAE.[28,54] Furthermore, an anisotropy factor of 5.9 is reached, which has not been reported for conductivities for P(NDI2OD-T_2) so far.

However, despite optimized procedures for vapor doping and high conductivities, TDAE seems to be not a very good dopant for P(NDI2OD-T2). This seems to have several reasons. (1) One reason might be that the conductivity reaches an intrinsic limit of P(NDI2OD-T_2) doping due to the strong localization of charges caused by the strong donor-acceptor character of this polymer.[38] This is corroborated by the electrochemical data which give clear evidence for mixed valence conductivity with discrete redox states. The localization of the charges is enhanced by the large dihedral angle between the naphthalenediimide and the bithiophene. Replacement of bithiophene with bithiazole was for example shown to reduce the torsional angle and increase conductivity.[55] Recently, several examples showed improved miscibility by polar side chains or kinks in the polymer structure.[32,37,64]

(2) Another reason might be that TDAE is not strong enough in terms of reducing capability. Cyclic voltammetry studies of TDAE in acetonitrile gave reversible oxidation waves for TDAE to $TDAE^{\bullet+}$ and $TDAE^{2+}$ with half wave potentials of -0.68 and -0.53 V vs. SCE which would result in -1.08 V and -0.93 V vs. Fc/Fc^{+}.[39,65,66] That means the first oxidation of TDAE fits to the first reduction of P(NDI2OD-T_2).When the films are put into the heated TDAE dish, the TDAE evaporates and condenses on the polymer films. As an excess of TDAE is present, P(NDI2OD-T_2) seems to be reduced the radical-anion to a certain extent and is electroneutralized by the $TDAE^{\bullet+}$ radical cation. This is in line with a pronounced radical anion band in presence of TDAE, as it could be shown in literature.[54]

(3) The third possibility is related to the high volatility of TDAE dopant molecules that leave the films after doping. As soon as the samples are removed from the TADE vapor, they seem to dedope as indicated by the colour change of the films. This might be explained by the high vapor pressure of TDAE (boiling point around 60 °C) or a slightly higher redox potential of $RR^{\bullet-} \rightarrow RR$. The latter is reasonable as the neutral band of P(NDI2OD-T_2) is rising after dedoping and no new bands are observed indicative of an irreversible secondary reaction (Figure S 17). TDAE might be too volatile to efficiently dope the polymer and stay in a doped state. This explanation is corroborated by the TEM data. TDAE doping of both form I and form II polymorphs of P(NDI2OD-T_2) results in a reduction of the unit cell parameters in the (a,c) plane and a substantial loss of π-stacking reflections. Moreover, order along the alkyl side chains is also disrupted as witnessed by a loss of higher order (*h00*) reflections. The reduction of the unit cell volume after doping suggests that there is no substantial amount of TDAE molecules present in the crystalline phase of P(NDI2OD-T_2). The final state of the film implies that most TDAE molecules that have doped the films in presence of dopant vapor, must have left the crystalline domains after removal of the sample from the dopant vapor atmosphere. This is corroborated by the UV–Vis results showing that the intensity of the radical-anion is lower in intensity after pumping the samples under vacuum (Figure S 17).

This situation reminds of the dedoping of iodine-doped polymers upon time as the doping is unstable.[67,68] Accordingly, it is proposed that the crystallites observed by TEM are essentially dedoped, whereas TDAE dopants may still be present in the amorphous phase. This would further be consistent with the rather low intensity of the radical-anion peaks in the UV–Vis spectra of TDAE-doped films as compared to the films doped electrochemically and the overall low conductivities measured in these samples.

Most remarkable is also the different impact of doping on the structures of form I and form II. After doping, the segregated stacking of form I is maintained but the interlayer order along alkyl side chains is strongly reduced (h00 with h≥2 are lost). Concerning form II, the situation is different. After doping with TDAE, form II films are transformed to form I. This implies a strong structural reorganization from mixed stacking (form II) to segregated stacking (form I). In other words, it implies that the π-stacking of the P(NDI2OD-T_2) chains is strongly perturbed upon doping. If the film is annealed to 300 °C for a second time, the UV–Vis spectrum suggests the recovery of form II (Figure). This suggests that no irreversible reaction with the dopant takes place as the polymorph can be recovered.

This is an interesting result as it shows that different polymorphs can respond differently to doping with TDAE in terms of structural reorganization.

To the best of our knowledge, it is the first evidence for the influence of polymorphism on doping in polymer semiconductors.

Conclusion.

Electrochemical and chemical doping of P(NDI2OD-T_2) and its regioirregular derivatives was investigated in detail. Organic electrochemical transistors were used to identify conduct-

ing states and first cycle effects could be elucidated. In contrast to classical semiconducting polymers, a maximum conductivity is only observed at a certain level of doping instead of a conductance plateau, which is in accordance with a mixed valence-conductivity model. N-DMBI and TDAE were used to chemically dope both regioregular and regioirregular P(NDI2OD-T_2) in isotropic spin-coated films and regioregular P(NDI2OD-T_2) in blade coated, large-scale aligned anisotropic films with well-defined morphologies. Maximum values up to $\sigma_{||} = 8.3 \cdot 10^{-3}\,S\,cm^{-1}$ were measured, which is among the highest values reported for P(NDI2OD-T_2) and slightly higher compared to literature doping with TDAE. Anisotropies around 5.9 indeed show a favoured charge transport along the blade coating direction over that perpendicular to it.

A reduced lamellar and backbone periodicity was observed in TEM after doping in BC/220 °C samples, while the lamellar order was reduced and no clear monoclinicity of the unit cell could be observed anymore. Additionally, the polymorph changes upon doping from form II back to form I. No coexistence of doped and undoped phases is found in the doped films and the overall alignment of the chains is only marginally perturbed by the doping process. All these findings claim for further *in situ* investigations of the doping process of n-type organic semiconducting polymers using GIXD or UV-vis spectroscopy in order to precise the mechanism of doping/dedoping with volatile dopants such as TDAE.

Our study helps further understanding the impact of doping on the polymer morphology, however, further studies are needed to fully understand the impact on the structure, e.g. reduction in backbone periodicity upon doping. Concluding, blade coating and doping of P(NDI2OD-T_2) with TDAE seem to be a suitable method for both achieving reasonable conductivities with high anisotropies and receiving detailed structural information on n-type doped semiconducting polymer films.

From this it is rather surprising that the polymer shows a measurable conductivity at all. The values in the manuscript are in the range of literature values. Wang et al. also showed the maximum conductivity at rather low radical-anion absorption, which is in line with the results here.[54] All the structures observed by TEM and characterized for their electrical conductivity corresponds most likely to a partially dedoped films, as TDAE leaves the samples in vacuum (present in the TEM and upon gold contact evaporation for electrical characterization).

It is still unclear if the conductivity around 10^{-3} S cm^{-1} is the maximum conductivity, as neither in literature nor by us a “fully doped” sample could be measured. On the one hand, the values shown on the slide are all around 10^{-3} S cm^{-1} but show substantial more radical-anion bands without vacuum. On the other hand, higher conductivity might be accessed when the radical-anion band exceeds the neutral band more than shown here. The search of stronger dopants in terms of reduction potential or less volatile dopants is presumably the key for successful, “irreversible doping” or “non-equilibrium doping”.

Experimental Section.

Cyclic voltammograms were recorded under Ar atmosphere in a three electrode setup with the polymer films deposited by spin coating on indium tin oxide (ITO) as working electrode, a platinum plate as counter electrode and a silver chloride coated silver wire as pseudo reference electrode. As electrolyte 0.1 M NBu_4PF_6 in acetonitrile was used, the scan rate was 20 mV s^{-1}. Experiments were performed with an Autolab PGSTAT101 potentiostat from Metrohm using the NOVA software. All potentials were rescaled to the formal potential of the redox couple Fc/Fc^+ (ferrocene/ferrocenium) as external standard.[69] UV-Vis spectra during cyclic voltammetry were taken with a Zeiss UV−vis spectrometer equipped with a MCS621 Vis II spectrometer and a CLH600F lamp. For in-situ conductance experiments inderdigitated platinum electrodes with the spincoated polymer film were used as working electrode. A constant bias of 10 mV was applied between the combs of the interdigitated electrode (distance between the combs is 5 µm) using a second potentiostat (µSTAT400, DropSens). The conductance profile of the polymers was calculated from the measured current between the two interdigitated Pt electrodes according to Ohm's law. Since the actually covered surface of the electrodes and the film thickness is very hard to determine, only the in-situ conductance profile no conductivity values of different films can be determined.

Atomic force microscopy was performed on a Bruker Dimension Icon AFM in tapping mode with HQ:NSC15/Al BS cantilevers from µMasch.

Preparation of aligned films by blade coating was performed on a Coatmaster 510 by Erichsen equipped with a blade tilted by 8 ° with respect to the substrate. The height was adjusted by micrometer screws to 100 µm above the substrate. Bladecoating was performed with a velocity of 1 mm s^{-1} at 80 °C. The polymer solution (c = 20 g l^{-1} in chlorobenzene) was applied at 80 °C with a preheated glass syringe.

Annealing of polymer films was done in an inert atmosphere using a THM 600 hot-stage (Linkam) controlled by a T95-PE temperature controller. Films were heated with a rate of 10 K min^{-1} to the indicated temperature, annealed for 5 min and slowly cooled to room temperature with a rate of 0.5 K min^{-1}.

Structural analysis: TEM: The preparation of the samples for TEM analysis involved four steps: i) floating the blade coated polymer layers on diluted HF solution (5 %) and transfer to TEM copper grids, ii) coating the films with a carbon layer deposited with an auto 306 Edwards evaporator, iii) annealing to 220 or 300 °C and iv) doping the TEM grids in the glove box with TDAE at 35 °C. To avoid sample ageing in ambient atmosphere, the TEM grids were mounted on the TEM sample holder inside the glove box and the holder was then transferred to the TEM in an air-tight container. The samples were only swiftly exposed to air (1-2 s) just before introducing the sample holder into the TEM. TEM was performed in the bright field and diffraction modes using a CM12 Philips microscope equipped with an MVIII (Soft Imaging System) Charge Coupled Device camera. Beam exposure was set to a minimum using the low dose system. TEM grids with a thin film of oriented PTFE films were further superposed with the P(NDI2OD-T_2) samples to serve as a reference for the calibration of reticular distances.

Doping: N-DMBI was synthesized according to procedures published in literature.[29,30] 4-(dimethylamino)benzaldehyde (0.150 g, 1.00 mmol, 1 eq.) and N,N-dimethyl-*o*-phenylenediamine (0.138 g, 1.01 mmol, 1.01 eq.) were dissolved in MeOH (2 ml) in a Schlenk tube. Glacial acetic acid (50 µl, cat.) was added and the solution was sonicated for 2 h. After freezing with liquid nitrogen and heating again to room temperature, a white precipitate was observed, which was then separated. Recrystallization from MeOH:H_2O (1:1, *v:v*, 22 ml) yielded N-DMBI as white, needle-like crystals (14 mg, 52.4 µmol, 5 %).

^{1}H NMR (250 MHz, $CDCl_3$): δ = 7.4–7.38 (m, 2H), 6.81–6.66 (m, 4H), 6.48–6.36 (m, 2H), 4.79 (s, 1H), 3.00 (s, 6H), 2.56 (s, 6H) ppm.

^{13}C NMR (63 MHz, $CDCl_3$): δ = 151.4, 142.4, 129.8, 126.2, 119.2, 112.2, 105.7, 94.0, 40.7, 33.2 ppm.

Isotropic P(NDI2OD-T_2)/N-DMBI blend films (RR: $\overline{M_n}$ = 18 kg mol^{-1}, PDI = 1.7, 1,2,4-trichlorobenzene HT-SEC (160 °C) calibrated vs. PS standards) were prepared by mixing aliquots of the polymer (3.33 g l^{-1} $CHCl_3$) and N-DMBI (3 g l^{-1} $CHCl_3$) and spin coating afterward in a N_2 filled glove box. The doping reaction was induced by heating at 55 °C for 3 h in inert atmosphere. RI(70:30) ($\overline{M_n}$ = 25 kg mol^{-1}, PDI = 1.7), RI(47:53) ($\overline{M_n}$ = 36 kg mol^{-1}, PDI = 1.9) and RI(24:76) ($\overline{M_n}$ = 11 kg mol^{-1}, PDI = 1.3) blends with N-DMBI were prepared accordingly.

TDAE was purchased from Ark Pharm, Inc. and was used as received. Vapor doping of P(NDI2OD-T_2) ($\overline{M_n}$ = 18 kg mol^{-1}, PDI = 1.7) was done by blade coating the pure polymer from 20 g l^{-1} CB at 80 °C, a blade height of 100 µm and 1 mm s^{-1} on cleaned glass substrates. The solution was not cooled down and was prepared beforehand by dissolving the polymer over night at 80 °C. In a glove box, TDAE (100 µl) was put in a closed Petri dish (V = 80 ml, d = 8 cm) and the substrates were fixed on top of the petri dish to expose the films to the TDAE vapor for the indicated time. For a higher vapor pressure, the Petri dish was put on a hot plate at 35 °C. Spin coating and vapor doping was done for all polymers with $CHCl_3$ at a concentration of 3 g l^{-1}.

Conductivity measurements:

Four equally distanced Au contacts ($d_{electrode}$ = 30 nm, $l_{channel}$ = 450 µm, $w_{channel}$ = 10 mm) were patterned on top of the doped films with a UNIVEX 350 G evaporation chamber by Oerlikon Leybold Vacuum at pressures below 10^{-6} mbar. Two sets of lines are parallel and perpendicular to the blade coating direction, respectively. Four-line electrical measurements

were done inside a nitrogen filled glove box using an EP 6 Probe Station from Süss MicroTec and a Keithley 2636 SourceMeter. The contact resistances are eliminated by applying a current at the outer lines and measurement of the voltage at the inner lines. The conductivity is calculated as follows:

$$\sigma = \frac{l_{\text{channel}}}{R \cdot w_{\text{channel}} \cdot d_{\text{film}}} \quad (1)$$

Film thicknesses d_{film} were determined by scratching the film from the substrate with a cannula and measuring the height difference at the edge between film and substrate by AFM.

Associated content.

Supporting information.

Author information.

Corresponding author.

*(S.L.) E-mail: sabine.ludwigs@ipoc.uni-stuttgart.de.

Acknowledgements.

Technical support from M. Schmutz and C. Blanck (TEM platform) is gratefully acknowledged. VV and VU acknowledge financial support through Idex Attractivité and IRTG grants, respectively. MB thanks ANR for financial support through grant ANR-17-CE05-0012 and CNRS through grant PEPS Energy Thermobody.

Y.M.G. thanks the Carl-Zeiss-Stiftung for a PhD scholarship.

References.

(1) Dubey, N.; Leclerc, M. Conducting Polymers: Efficient Thermoelectric Materials. *J. Polym. Sci. Part B Polym. Phys.* **2011**, *49* (7), 467–475. https://doi.org/10.1002/polb.22206.

(2) McGrail, B. T.; Sehirlioglu, A.; Pentzer, E. Polymer Composites for Thermoelectric Applications. *Angew. Chemie Int. Ed.* **2015**, *54* (6), 1710–1723. https://doi.org/10.1002/anie.201408431.

(3) Bubnova, O.; Crispin, X. Towards Polymer-Based Organic Thermoelectric Generators. *Energy Environ. Sci.* **2012**, *5* (11), 9345. https://doi.org/10.1039/c2ee22777k.

(4) Guo, Y.; Sato, W.; Inoue, K.; Zhang, W.; Yu, G.; Nakamura, E. N-Type Doping for Efficient Polymeric Electron-Transporting Layers in Perovskite Solar Cells. *J. Mater. Chem. A* **2016**, *4* (48), 18852–18856. https://doi.org/10.1039/C6TA08526A.

(5) Cho, N.; Yip, H.-L.; Davies, J. A.; Kazarinoff, P. D.; Zeigler, D. F.; Durban, M. M.; Segawa, Y.; O'Malley, K. M.; Luscombe, C. K.; Jen, A. K.-Y. In-Situ Crosslinking and n-Doping of Semiconducting Polymers and Their Application as Efficient Electron-Transporting Materials in Inverted Polymer Solar Cells. *Adv. Energy Mater.* **2011**, *1* (6), 1148–1153. https://doi.org/10.1002/aenm.201100429.

(6) Chen, L.-M.; Xu, Z.; Hong, Z.; Yang, Y. Interface Investigation and Engineering – Achieving High Performance Polymer Photovoltaic Devices. *J. Mater. Chem.* **2010**, *20* (13), 2575–2598. https://doi.org/10.1039/b925382c.

(7) Yip, H.-L.; Jen, A. K. Y. Recent Advances in Solution-Processed Interfacial Materials for Efficient and Stable Polymer Solar Cells. *Energy Environ. Sci.* **2012**, *5* (3), 5994. https://doi.org/10.1039/c2ee02806a.

(8) Zhou, H.; Zhang, Y.; Mai, C.-K.; Collins, S. D.; Nguyen, T.-Q.; Bazan, G. C.; Heeger,

A. J. Conductive Conjugated Polyelectrolyte as Hole-Transporting Layer for Organic Bulk Heterojunction Solar Cells. *Adv. Mater.* **2014**, *26* (5), 780–785. https://doi.org/10.1002/adma.201302845.

(9) Snyder, G. J.; Toberer, E. S. Complex Thermoelectric Materials. *Nat. Mater.* **2008**, *7* (2), 105–114. https://doi.org/10.1038/nmat2090.

(10) Zhang, X.; Zhao, L.-D. Thermoelectric Materials: Energy Conversion between Heat and Electricity. *J. Mater.* **2015**, *1* (2), 92–105. https://doi.org/10.1016/j.jmat.2015.01.001.

(11) Steyrleuthner, R.; Schubert, M.; Howard, I.; Klaumünzer, B.; Schilling, K.; Chen, Z.; Saalfrank, P.; Laquai, F.; Facchetti, A.; Neher, D. Aggregation in a High-Mobility n-Type Low-Bandgap Copolymer with Implications on Semicrystalline Morphology. *J. Am. Chem. Soc.* **2012**, *134* (44), 18303–18317. https://doi.org/10.1021/ja306844f.

(12) Schubert, M.; Dolfen, D.; Frisch, J.; Roland, S.; Steyrleuthner, R.; Stiller, B.; Chen, Z.; Scherf, U.; Koch, N.; Facchetti, A.; et al. Influence of Aggregation on the Performance of All-Polymer Solar Cells Containing Low-Bandgap Naphthalenediimide Copolymers. *Adv. Energy Mater.* **2012**, *2* (3), 369–380. https://doi.org/10.1002/aenm.201100601.

(13) Liu, Y.; Zhao, J.; Li, Z.; Mu, C.; Ma, W.; Hu, H.; Jiang, K.; Lin, H.; Ade, H.; Yan, H. Aggregation and Morphology Control Enables Multiple Cases of High-Efficiency Polymer Solar Cells. *Nat. Commun.* **2014**, *5* (1), 5293. https://doi.org/10.1038/ncomms6293.

(14) Nahid, M. M.; Welford, A.; Gann, E.; Thomsen, L.; Sharma, K. P.; McNeill, C. R. Nature and Extent of Solution Aggregation Determines the Performance of P(NDI2OD-T2) Thin-Film Transistors. *Adv. Electron. Mater.* **2018**, *4* (4), 1700559. https://doi.org/10.1002/aelm.201700559.

(15) Trefz, D.; Gross, Y. M.; Dingler, C.; Tkachov, R.; Hamidi-Sakr, A.; Kiriy, A.; McNeill, C. R.; Brinkmann, M.; Ludwigs, S. Tuning Orientational Order of Highly Aggregating P(NDI2OD-T2) by Solvent Vapor Annealing and Blade Coating. *Macromolecules* **2019**, *52* (1), 43–54. https://doi.org/10.1021/acs.macromol.8b02176.

(16) Steyrleuthner, R.; Di Pietro, R.; Collins, B. A.; Polzer, F.; Himmelberger, S.; Schubert, M.; Chen, Z.; Zhang, S.; Salleo, A.; Ade, H.; et al. The Role of Regioregularity, Crystallinity, and Chain Orientation on Electron Transport in a High-Mobility n-Type Copolymer. *J. Am. Chem. Soc.* **2014**, *136* (11), 4245–4256. https://doi.org/10.1021/ja4118736.

(17) Gross, Y. M.; Trefz, D.; Tkachov, R.; Untilova, V.; Brinkmann, M.; Schulz, G. L.; Ludwigs, S. Tuning Aggregation by Regioregularity for High-Performance n-Type P(NDI2OD-T2) Donor–Acceptor Copolymers. *Macromolecules* **2017**, *50* (14), 5353–5366. https://doi.org/10.1021/acs.macromol.7b01386.

(18) Crossland, E. J. W.; Tremel, K.; Fischer, F.; Rahimi, K.; Reiter, G.; Steiner, U.; Ludwigs, S. Anisotropic Charge Transport in Spherulitic Poly(3-Hexylthiophene) Films. *Adv. Mater.* **2012**, *24* (6), 839–844. https://doi.org/10.1002/adma.201104284.

(19) Fischer, F. S. U.; Tremel, K.; Sommer, M.; Crossland, E. J. C.; Ludwigs, S. Directed Crystallization of Poly(3-Hexylthiophene) in Micrometre Channels under Confinement and in Electric Fields. *Nanoscale* **2012**, *4*, 2138. https://doi.org/10.1039/c2nr12037b.

(20) Tremel, K.; Fischer, F. S. U.; Kayunkid, N.; Di Pietro, R.; Tkachov, R.; Kiriy, A.; Neher, D.; Ludwigs, S.; Brinkmann, M. Charge Transport Anisotropy in Highly Oriented Thin Films of the Acceptor Polymer P(NDI2OD-T2). *Adv. Energy Mater.* **2014**, *4* (10), 1301659. https://doi.org/10.1002/aenm.201301659.

(21) Hamidi-Sakr, A.; Biniek, L.; Fall, S.; Brinkmann, M. Precise Control of Lamellar

Thickness in Highly Oriented Regioregular Poly(3-Hexylthiophene) Thin Films Prepared by High-Temperature Rubbing: Correlations with Optical Properties and Charge Transport. *Adv. Funct. Mater.* **2016**, *26* (3), 408–420. https://doi.org/10.1002/adfm.201504096.

(22) Bucella, S. G.; Luzio, A.; Gann, E.; Thomsen, L.; McNeill, C. R.; Pace, G.; Perinot, A.; Chen, Z.; Facchetti, A.; Caironi, M. Macroscopic and High-Throughput Printing of Aligned Nanostructured Polymer Semiconductors for MHz Large-Area Electronics. *Nat. Commun.* **2015**, *6*, 8394. https://doi.org/10.1038/ncomms9394.

(23) Pan, G.; Chen, F.; Hu, L.; Zhang, K.; Dai, J.; Zhang, F. Effective Controlling of Film Texture and Carrier Transport of a High-Performance Polymeric Semiconductor by Magnetic Alignment. *Adv. Funct. Mater.* **2015**, *25* (32), 5126–5133. https://doi.org/10.1002/adfm.201500643.

(24) Hamidi-Sakr, A.; Biniek, L.; Bantignies, J.-L.; Maurin, D.; Herrmann, L.; Leclerc, N.; Lévêque, P.; Vijayakumar, V.; Zimmermann, N.; Brinkmann, M. A Versatile Method to Fabricate Highly In-Plane Aligned Conducting Polymer Films with Anisotropic Charge Transport and Thermoelectric Properties: The Key Role of Alkyl Side Chain Layers on the Doping Mechanism. *Adv. Funct. Mater.* **2017**, *27* (25), 1700173. https://doi.org/10.1002/adfm.201700173.

(25) Chen, Z.; Zheng, Y.; Yan, H.; Facchetti, A. Naphthalenedicarboximide- vs Perylenedicarboximide-Based Copolymers. Synthesis and Semiconducting Properties in Bottom-Gate N-Channel Organic Transistors. *J. Am. Chem. Soc.* **2009**, *131* (1), 8–9. https://doi.org/10.1021/ja805407g.

(26) Jung, J. W.; Jo, J. W.; Chueh, C.-C.; Liu, F.; Jo, W. H.; Russell, T. P.; Jen, A. K.-Y. Fluoro-Substituted n-Type Conjugated Polymers for Additive-Free All-Polymer Bulk Heterojunction Solar Cells with High Power Conversion Efficiency of 6.71%. *Adv.*

Mater. **2015**, *27* (21), 3310–3317. https://doi.org/10.1002/adma.201501214.

(27) Trefz, D.; Ruff, A.; Tkachov, R.; Wieland, M.; Goll, M.; Kiriy, A.; Ludwigs, S. Electrochemical Investigations of the N-Type Semiconducting Polymer P(NDI2OD-T2) and Its Monomer: New Insights in the Reduction Behavior. *J. Phys. Chem. C* **2015**, *119* (40), 22760–22771. https://doi.org/10.1021/acs.jpcc.5b05756.

(28) Schlitz, R. A.; Brunetti, F. G.; Glaudell, A. M.; Miller, P. L.; Brady, M. A.; Takacs, C. J.; Hawker, C. J.; Chabinyc, M. L. Solubility-Limited Extrinsic n-Type Doping of a High Electron Mobility Polymer for Thermoelectric Applications. *Adv. Mater.* **2014**, *26* (18), 2825–2830. https://doi.org/10.1002/adma.201304866.

(29) Zhu, X.-Q.; Zhang, M.-T.; Yu, A.; Wang, C.-H.; Cheng, J.-P. Hydride, Hydrogen Atom, Proton, and Electron Transfer Driving Forces of Various Five-Membered Heterocyclic Organic Hydrides and Their Reaction Intermediates in Acetonitrile. *J. Am. Chem. Soc.* **2008**, *130* (8), 2501–2516. https://doi.org/10.1021/ja075523m.

(30) Naab, B. D.; Guo, S.; Olthof, S.; Evans, E. G. B.; Wei, P.; Millhauser, G. L.; Kahn, A.; Barlow, S.; Marder, S. R.; Bao, Z. Mechanistic Study on the Solution-Phase n-Doping of 1,3-Dimethyl-2-Aryl-2,3-Dihydro-1H -Benzoimidazole Derivatives. *J. Am. Chem. Soc.* **2013**, *135* (40), 15018–15025. https://doi.org/10.1021/ja403906d.

(31) Liang, Y.; Chen, Z.; Jing, Y.; Rong, Y.; Facchetti, A.; Yao, Y. Heavily N-Dopable π-Conjugated Redox Polymers with Ultrafast Energy Storage Capability. *J. Am. Chem. Soc.* **2015**, *137* (15), 4956–4959. https://doi.org/10.1021/jacs.5b02290.

(32) Liu, J.; Qiu, L.; Alessandri, R.; Qiu, X.; Portale, G.; Dong, J. J.; Talsma, W.; Ye, G.; Sengrian, A. A.; Souza, P. C. T.; et al. Enhancing Molecular N-Type Doping of Donor–Acceptor Copolymers by Tailoring Side Chains. *Adv. Mater.* **2018**, *30* (7), 1–9. https://doi.org/10.1002/adma.201704630.

(33) Wei, P.; Oh, J. H.; Dong, G.; Bao, Z. Use of a 1 H -Benzoimidazole Derivative as an n -Type Dopant and To Enable Air-Stable Solution-Processed n -Channel Organic Thin-Film Transistors. *J. Am. Chem. Soc.* **2010**, *132* (26), 8852–8853. https://doi.org/10.1021/ja103173m.

(34) Zhou, Y.; Fuentes-Hernandez, C.; Shim, J.; Meyer, J.; Giordano, A. J.; Li, H.; Winget, P.; Papadopoulos, T.; Cheun, H.; Kim, J.; et al. A Universal Method to Produce Low-Work Function Electrodes for Organic Electronics. *Science (80-.).* **2012**, *336* (6079), 327–332. https://doi.org/10.1126/science.1218829.

(35) Fabiano, S.; Braun, S.; Liu, X.; Weverberghs, E.; Gerbaux, P.; Fahlman, M.; Berggren, M.; Crispin, X. Poly(Ethylene Imine) Impurities Induce n-Doping Reaction in Organic (Semi)Conductors. *Adv. Mater.* **2014**, *26* (34), 6000–6006. https://doi.org/10.1002/adma.201401986.

(36) Liu, J.; Qiu, L.; Portale, G.; Koopmans, M.; ten Brink, G.; Hummelen, J. C.; Koster, L. J. A. N-Type Organic Thermoelectrics: Improved Power Factor by Tailoring Host–Dopant Miscibility. *Adv. Mater.* **2017**, *29* (36). https://doi.org/10.1002/adma.201701641.

(37) Kiefer, D.; Giovannitti, A.; Sun, H.; Biskup, T.; Hofmann, A.; Koopmans, M.; Cendra, C.; Weber, S.; Anton Koster, L. J.; Olsson, E.; et al. Enhanced N-Doping Efficiency of a Naphthalenediimide-Based Copolymer through Polar Side Chains for Organic Thermoelectrics. *ACS Energy Lett.* **2018**, *3* (2), 278–285. https://doi.org/10.1021/acsenergylett.7b01146.

(38) Naab, B. D.; Gu, X.; Kurosawa, T.; To, J. W. F.; Salleo, A.; Bao, Z. Role of Polymer Structure on the Conductivity of N-Doped Polymers. *Adv. Electron. Mater.* **2016**, *2* (5), 1600004. https://doi.org/10.1002/aelm.201600004.

(39) Cardona, C. M.; Li, W.; Kaifer, A. E.; Stockdale, D.; Bazan, G. C. Electrochemical Considerations for Determining Absolute Frontier Orbital Energy Levels of Conjugated Polymers for Solar Cell Applications. *Adv. Mater.* **2011**, *23* (20), 2367–2371. https://doi.org/10.1002/adma.201004554.

(40) Heinze, J.; Frontana-Uribe, B. A.; Ludwigs, S. Electrochemistry of Conducting Polymers—Persistent Models and New Concepts. *Chem. Rev.* **2010**, *110* (8), 4724–4771. https://doi.org/10.1021/cr900226k.

(41) Jespersen, K. G.; Beenken, W. J. D.; Zaushitsyn, Y.; Yartsev, A.; Andersson, M.; Pullerits, T.; Sundström, V. The Electronic States of Polyfluorene Copolymers with Alternating Donor-Acceptor Units. *J. Chem. Phys.* **2004**, *121* (24), 12613–12617. https://doi.org/10.1063/1.1817873.

(42) Bernards, D. A.; Malliaras, G. G. Steady-State and Transient Behavior of Organic Electrochemical Transistors. *Adv. Funct. Mater.* **2007**, *17* (17), 3538–3544. https://doi.org/10.1002/adfm.200601239.

(43) Link, S.; Richter, T.; Yurchenko, O.; Heinze, J.; Ludwigs, S. Electrochemical Behavior of Electropolymerized and Chemically Synthesized Hyperbranched Polythiophenes. *J. Phys. Chem. B* **2010**, *114* (33), 10703–10708. https://doi.org/10.1021/jp1035629.

(44) Tremel, K.; Ludwigs, S. Morphology of P3HT in Thin Films in Relation to Optical and Electrical Properties. In *P3HT Revisited - from Molecular Scale to Solar Cell Devices*; Ludwigs, S., Ed.; Springer-Verlag Berlin Heidelberg, 2014; pp 39–82.

(45) Yurchenko, O.; Heinze, J.; Ludwigs, S. Electrochemically Induced Formation of Independent Conductivity Regimes in Polymeric Tetraphenylbenzidine Systems. *ChemPhysChem* **2010**, *11*, 1637–1640. https://doi.org/10.1002/cphc.201000131.

(46) Chidsey, C. E. D.; Murray, R. W. Redox Capacity and Direct Current Electron

Conductivity in Electroactive Materials. *J. Phys. Chem.* **1986**, *90* (7), 1479–1484. https://doi.org/10.1021/j100398a051.

(47) Caironi, M.; Bird, M.; Fazzi, D.; Chen, Z.; Di Pietro, R.; Newman, C.; Facchetti, A.; Sirringhaus, H. Very Low Degree of Energetic Disorder as the Origin of High Mobility in an N-Channel Polymer Semiconductor. *Adv. Funct. Mater.* **2011**, *21* (17), 3371–3381. https://doi.org/10.1002/adfm.201100592.

(48) D'Innocenzo, V.; Luzio, A.; Petrozza, A.; Fazzi, D.; Caironi, M. Nature of Charge Carriers in a High Electron Mobility Naphthalenediimide Based Semiconducting Copolymer. *Adv. Funct. Mater.* **2014**, *24* (35), 5584–5593. https://doi.org/10.1002/adfm.201400394.

(49) Valdes, L. B. Resistivity Measurements on Germanium for Transistors. *Proc. I.R.E.* **1954**, *42*, 420–427.

(50) Allemand, P.-M.; Khemani, K. C.; Koch, A.; Wudl, F.; Holczer, K.; Donovan, S.; Gruner, G.; Thompson, J. D. Organic Molecular Soft Ferromagnetism in a Fullerene C60. *Science (80-.).* **1991**, *253*, 301–303. https://doi.org/10.1126/science.253.5017.301.

(51) Lindell, L.; Burquel, A.; Jakobsson, F. L. E.; Lemaur, V.; Berggren, M.; Lazzaroni, R.; Cornil, J.; Salaneck, W. R.; Crispin, X. Transparent, Plastic, Low-Work-Function Poly(3,4-Ethylenedioxythiophene) Electrodes. *Chem. Mater.* **2006**, *18* (18), 4246–4252. https://doi.org/10.1021/cm061081m.

(52) Bagnato, J. D.; Shum, W. W.; Strohmeier, M.; Grant, D. M.; Arif, A. M.; Miller, J. S. The Structure of Fractionally Charged Tetracyanobenzenen- Present in [TCNB]32-. *Angew. Chemie - Int. Ed.* **2006**, *45* (32), 5322–5326. https://doi.org/10.1002/anie.200601070.

(53) Naab, B. D.; Zhang, S.; Vandewal, K.; Salleo, A.; Barlow, S.; Marder, S. R.; Bao, Z. Effective Solution- and Vacuum-Processed n-Doping by Dimers of Benzimidazoline Radicals. *Adv. Mater.* **2014**, *26* (25), 4268–4272. https://doi.org/10.1002/adma.201400668.

(54) Wang, S.; Sun, H.; Ail, U.; Vagin, M.; Persson, P. O. Å.; Andreasen, J. W.; Thiel, W.; Berggren, M.; Crispin, X.; Fazzi, D.; et al. Thermoelectric Properties of Solution-Processed n-Doped Ladder-Type Conducting Polymers. *Adv. Mater.* **2016**, *28* (48), 10764–10771. https://doi.org/10.1002/adma.201603731.

(55) Wang, S.; Sun, H.; Erdmann, T.; Wang, G.; Fazzi, D.; Lappan, U.; Puttisong, Y.; Chen, Z.; Berggren, M.; Crispin, X.; et al. A Chemically Doped Naphthalenediimide-Bithiazole Polymer for n-Type Organic Thermoelectrics. *Adv. Mater.* **2018**, *30* (31), 1801898. https://doi.org/10.1002/adma.201801898.

(56) Brinkmann, M.; Gonthier, E.; Bogen, S.; Tremel, K.; Ludwigs, S.; Hufnagel, M.; Sommer, M. Segregated versus Mixed Interchain Stacking in Highly Oriented Films of Naphthalene Diimide Bithiophene Copolymers. *ACS Nano* **2012**, *6* (11), 10319–10326. https://doi.org/10.1021/nn304213h.

(57) Brinkmann, M.; Wittmann, J.-C.; Barthel, M.; Hanack, M.; Chaumont, C. Highly Ordered Titanyl Phthalocyanine Films Grown by Directional Crystallization on Oriented Poly(Tetrafluoroethylene) Substrate. *Chem. Mater.* **2002**, *14* (2), 904–914. https://doi.org/10.1021/cm011241o.

(58) Schuettfort, T.; Huettner, S.; Lilliu, S.; Macdonald, J. E.; Thomsen, L.; McNeill, C. R. Surface and Bulk Structural Characterization of a High-Mobility Electron-Transporting Polymer. *Macromolecules* **2011**, *44* (6), 1530–1539. https://doi.org/10.1021/ma102451b.

(59) Schuettfort, T.; Thomsen, L.; McNeill, C. R. Observation of a Distinct Surface Molecular Orientation in Films of a High Mobility Conjugated Polymer. *J. Am. Chem. Soc.* **2013**, *135* (3), 1092–1101. https://doi.org/10.1021/ja310240q.

(60) Giussani, E.; Fazzi, D.; Brambilla, L.; Caironi, M.; Castiglioni, C. Molecular Level Investigation of the Film Structure of a High Electron Mobility Copolymer via Vibrational Spectroscopy. *Macromolecules* **2013**, *46* (7), 2658–2670. https://doi.org/10.1021/ma302664s.

(61) Giussani, E.; Brambilla, L.; Fazzi, D.; Sommer, M.; Kayunkid, N.; Brinkmann, M.; Castiglioni, C. Structural Characterization of Highly Oriented Naphthalene-Diimide-Bithiophene Copolymer Films via Vibrational Spectroscopy. *J. Phys. Chem. B* **2015**, *119* (5), 2062–2073. https://doi.org/10.1021/jp511451s.

(62) Raos, G.; Famulari, A.; Marcon, V. Computational Reinvestigation of the Bithiophene Torsion Potential. *Chem. Phys. Lett.* **2003**, *379* (3–4), 364–372. https://doi.org/10.1016/j.cplett.2003.08.060.

(63) Fazzi, D.; Caironi, M.; Castiglioni., C. Quantum-Chemical Insights into the Prediction of Charge Transport Parameters for a Naphthalenetetracarboxydiimide-Based Copolymer with Enhanced Electron Mobility. *J. Am. Chem. Soc.* **2011**, *133* (47), 19056–19059. https://doi.org/10.1021/ja208824d.

(64) Shin, Y.; Massetti, M.; Komber, H.; Biskup, T.; Nava, D.; Lanzani, G.; Caironi, M.; Sommer, M. Improving Miscibility of a Naphthalene Diimide-Bithiophene Copolymer with n-Type Dopants through the Incorporation of “Kinked” Monomers. *Adv. Electron. Mater.* **2018**, *4* (10), 1700581. https://doi.org/10.1002/aelm.201700581.

(65) Wiberg, N. Tetraaminoethylenes as Strong Electron Donors. *Angew. Chemie Int. Ed. English* **1968**, *7* (10), 766–779. https://doi.org/10.1002/anie.196807661.

(66) Fox, J. R.; Foxman, B. M.; Guarrera, D.; Miller, J. S.; Calabrese, J. C.; Reis, A. H. Characterization of Novel TCNQ and TCNE 1:1 and 1:2 Salts of the Tetrakis(Dimethyamino)Ethylene Dication, [{(CH3)2N}2C?C{N(CH3)2}2]2+ . *J. Mater. Chem.* **1996**, *6* (10), 1627. https://doi.org/10.1039/jm9960601627.

(67) Loponen, M. T.; Taka, T.; Laakso, J.; Väkiparta, K.; Suuronen, K.; Valkeinen, P.; Österholm, J.-E. Doping and Dedoping Processes in Poly (3-Alkylthiophenes). *Synth. Met.* **1991**, *41* (1–2), 479–484. https://doi.org/10.1016/0379-6779(91)91111-M.

(68) Koizumi, H.; Dougauchi, H.; Ichikawa, T. Mechanism of Dedoping Processes of Conducting Poly(3-Alkylthiophenes). *J. Phys. Chem. B* **2005**, *109* (32), 15288–15290. https://doi.org/10.1021/jp051989k.

(69) Gritzner, G.; Kuta, J. Recommendations on Reporting Electrode Potentials in Nonaqueous Solvents. *Pure Appl. Chem.* **1984**, *56* (4), 461–466. https://doi.org/10.1351/pac198456040461.

Supporting Information

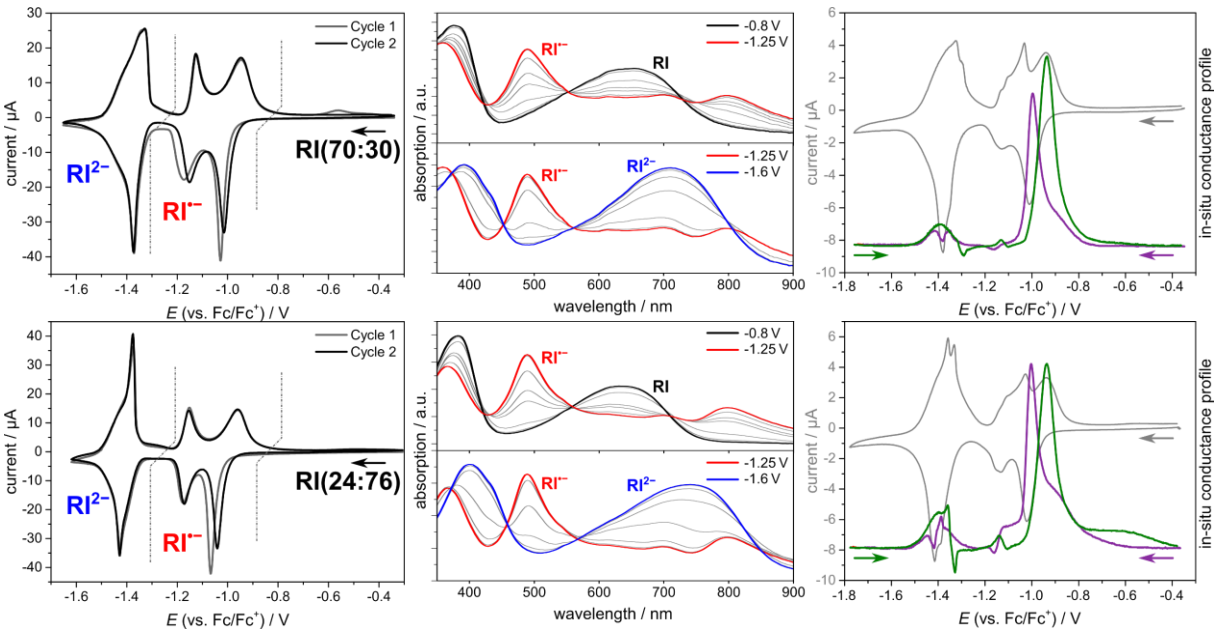

Figure S 1. Electrochemical characteristics of RI(70:30) (top) and RI(24:76) (bottom). Cyclic voltammograms were measured of films spin coated from $CHCl_3$ (c = 3 g/l) on ITO as working electrode in 0.1 M NBu_4PF_6/MeCN as electrolyte. Scan rate is 20 mV/s. UV-Vis spectra recorded during the forward scan in the 2nd cycle, the spectra are divided into the first (−0.8 to −1.25 V) and second (−1.25 to −1.6 V) reduction. In-situ conductance and cyclic voltammogram on interdigitated Pt electrodes. Purple is the forward and green the backward scan. The potential difference between the two combs is 10 mV. The measurements were performed in NBu_4PF_6/MeCN as electrolyte with a scan rate of 10 mV/s.

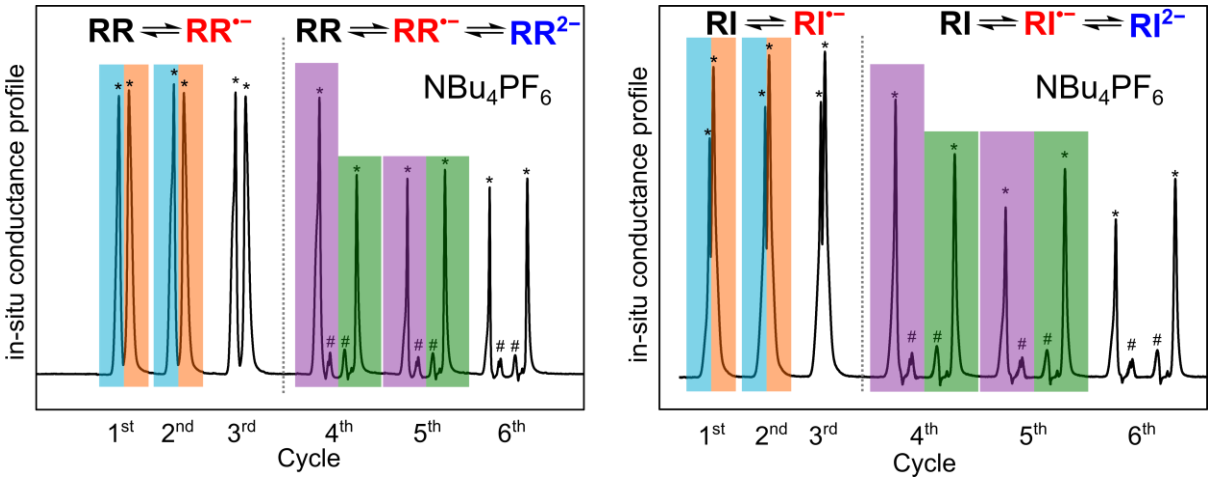

Figure S 2. Plots of the in-situ conductance as function of the cycles of RR and RI(47:53). During the first three cycles, the potential scan was reversed after the first reduction (around -1.1 V, *), and in the three subsequent cycles (4^{th}-6^{th} cycle), the polymer was fully reduced to the dianion (#). The highlighted color corresponds to the in-situ conductance curves presented in the main text in Figure 2.

The in-situ conductance was investigated at different vertex potentials. Specifically, a freshly prepared film was just reduced to the radical-anion for three times and then fully reduced to the dianion, which is shown in Figure 2 c) for RR. In this graph the course of the in-situ conductance of several consecutive measurements is plotted versus the measurement time, which is connected to the potential via the scan rate (10 mV/s). In the first three cycles the potential was turned before the second reduction, that is, the first six signals in Figure 2 belong to the first reduction and the associated reoxidation.

In the fourth cycle, RR was reduced twofold, i.e. to the dianion. Four peaks (highlighted by * and #) in the plot belong to this cycle, namely that of the first reduction (*), second reduction (#) and that of the two corresponding reoxidations. From this figure it is obvious that the in-situ conductance remains almost constant during the first three cycles and then drops after the polymer is reduced to the dianion for the first time. This suggests that a process during the second reduction causes the decrease in conductance. This process might be the incorporation of even more counter ions – in addition to the incorporation during the first reduction – and further swelling of the film, which might irreversibly decrease the in-situ conductance.

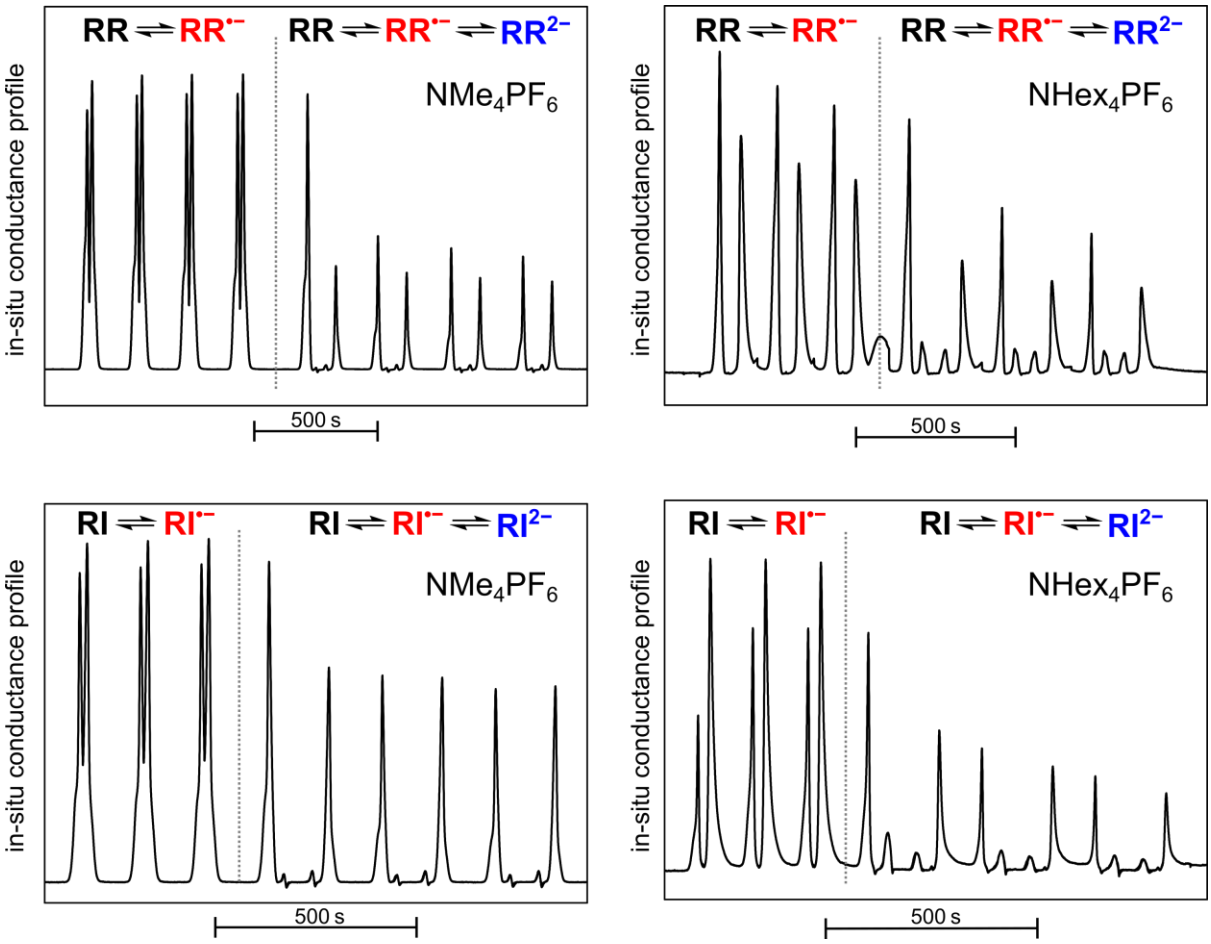

Figure S 3. In-situ conductance of RR and RI(47:53) films spin coated from $CHCl_3$ (c = 3 g/l) on inter-digitated Pt electrodes. The measurements were performed with the indicated conducting salt in MeCN as electrolyte with a scan rate of 10 mV/s. The in-situ conductance is plotted as function of the measurement time. During the first cycles, the potential was turned before the second reduction (around -1.1 V), and in subsequent cycles, the polymer was fully reduced to the dianion, as illustrated by the dotted line.

In-situ absorption spectroscopy of films following the peak trend of the 489 nm radical-anion band upon heating from RT with 1K/min up to 180°C clearly show that: (1) already at temperatures around 50 °C the 489 nm band constantly increases suggesting that the doping reaction is already happening at low temperatures and that (2) temperatures over 80°C reveal decreasing intensity of the 489 nm which might be due to dedoping.

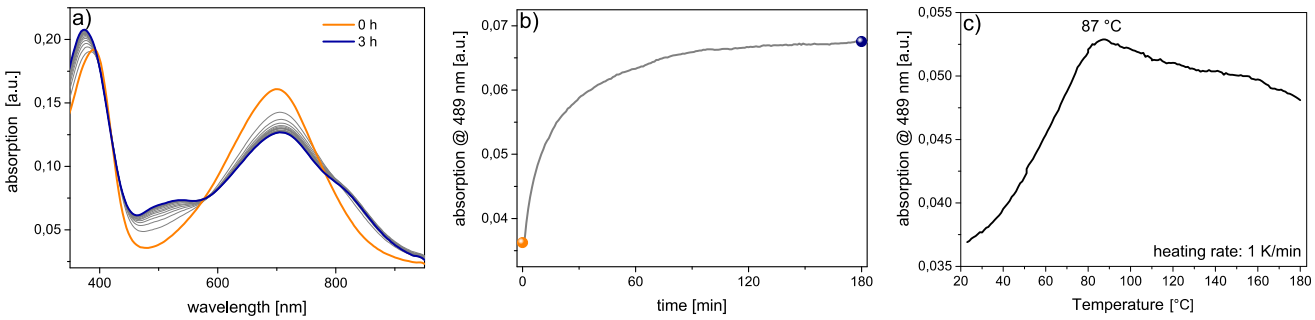

Figure S 4. a) UV-Vis absorption spectra during doping of a P(NDI2OD-T_2) film with 100 mol% N-DMBI at 55 °C for 3 h. Difference between the spectra is 10 min. b) Absorption intensities at 489 nm as function of doping time. The colored data points correspond to the absorption spectra shown on the left. c) Peaktrend during doping of a P(NDI2OD-T_2) film with 100 mol% N-DMBI at higher temperatures with a heating rate of 1 K min^{-1}.

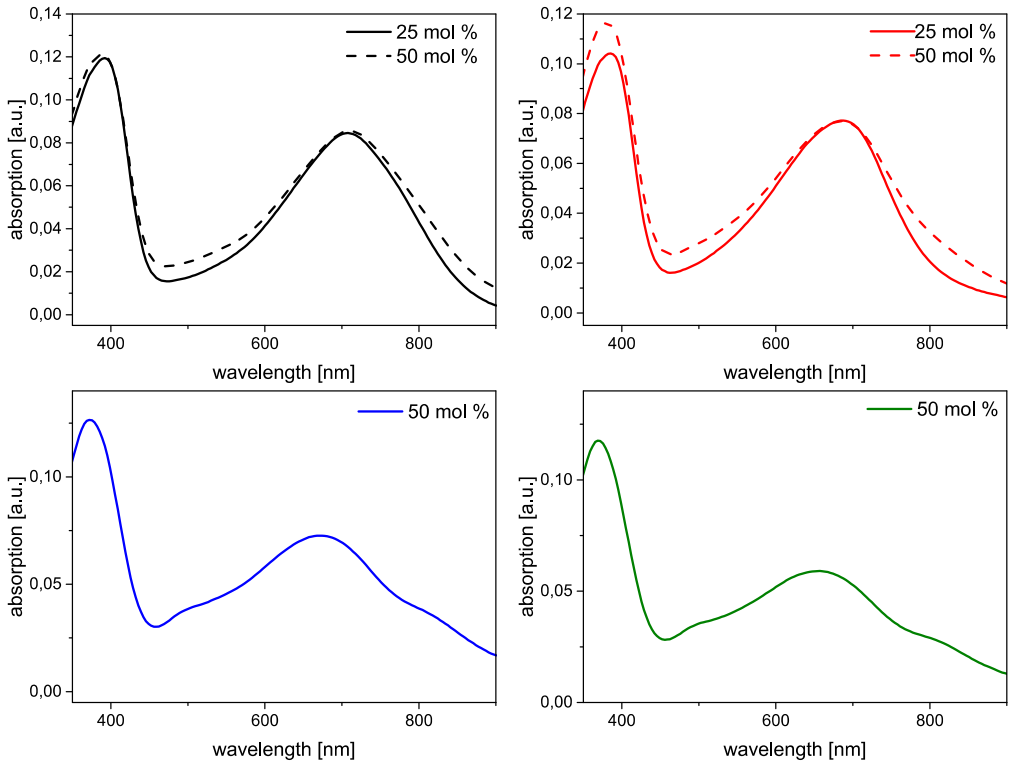

Figure S 5. Absorption spectroscopy of spin coated P(NDI2OD-T_2)/N-DMBI blends with different amounts of N-DMBI after temperature treatment at 55 °C for 3 h.. Black: RR, red: RI(70:30), blue: RI(47:53), green: RI(24:76).

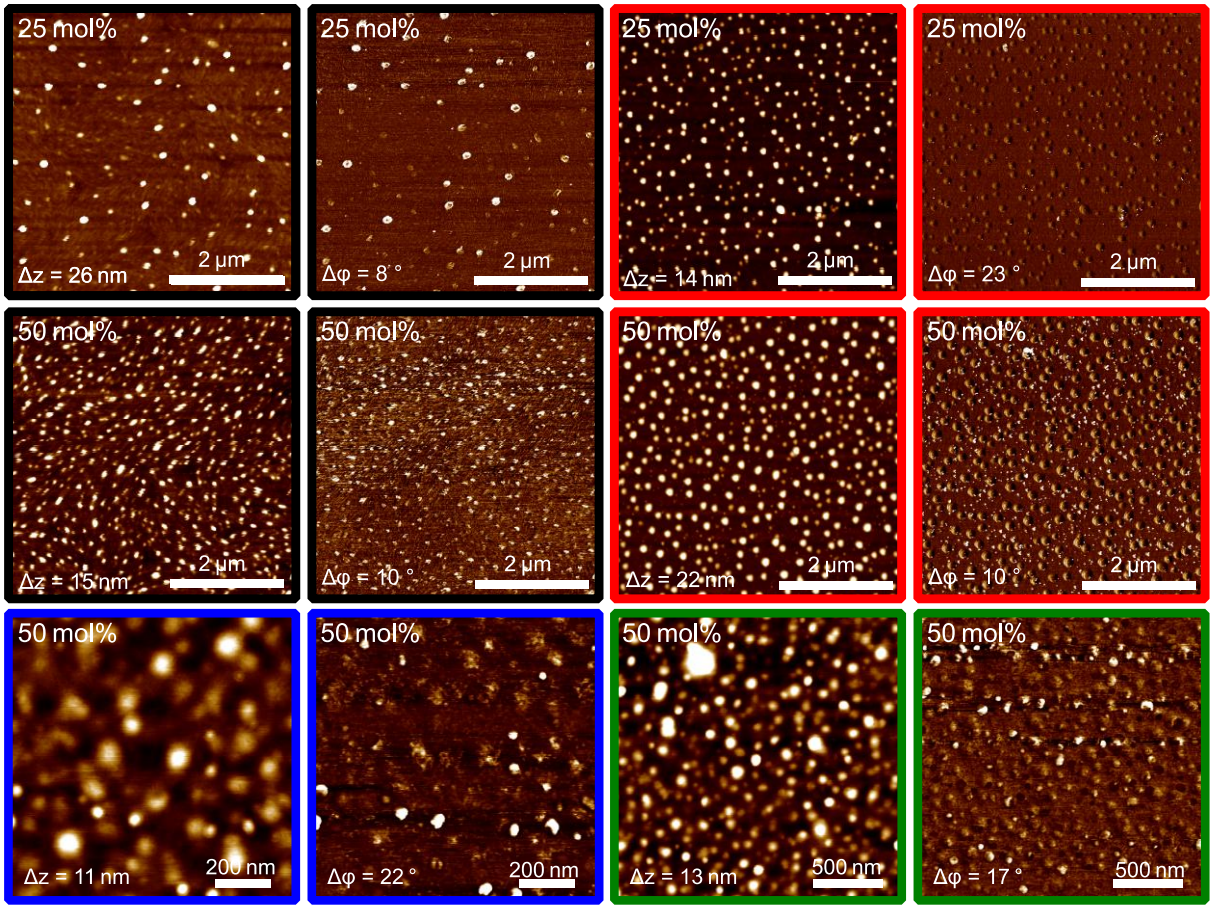

Figure S 6. AFM height and phase images obtained in tapping-mode of spin coated RR/N-DMBI (25 and 50 mol%) (black), RI(70:30)/N-DMBI (25 and 50 mol%) (red), RI(47:53)/N-DMBI (50 mol%) (blue) and RI(24:76)/N-DMBI (50 mol%) (green) thin films. Films were temperature treated for 3 h at 55 °C after spin coating to induce the doping reaction.

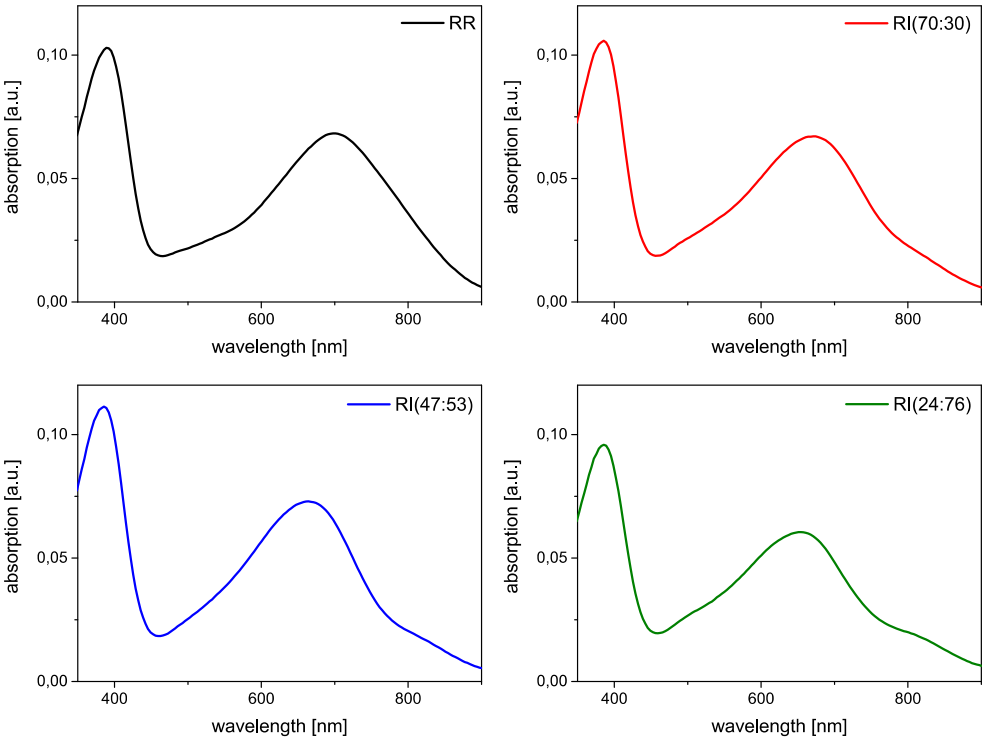

Figure S 7. Absorption spectroscopy of spin coated P(NDI2OD-T_2) films doped for 120 min in TDAE vapor at 35 °C. Black: RR, red: RI(70:30), blue: RI(47:53), green: RI(24:76).

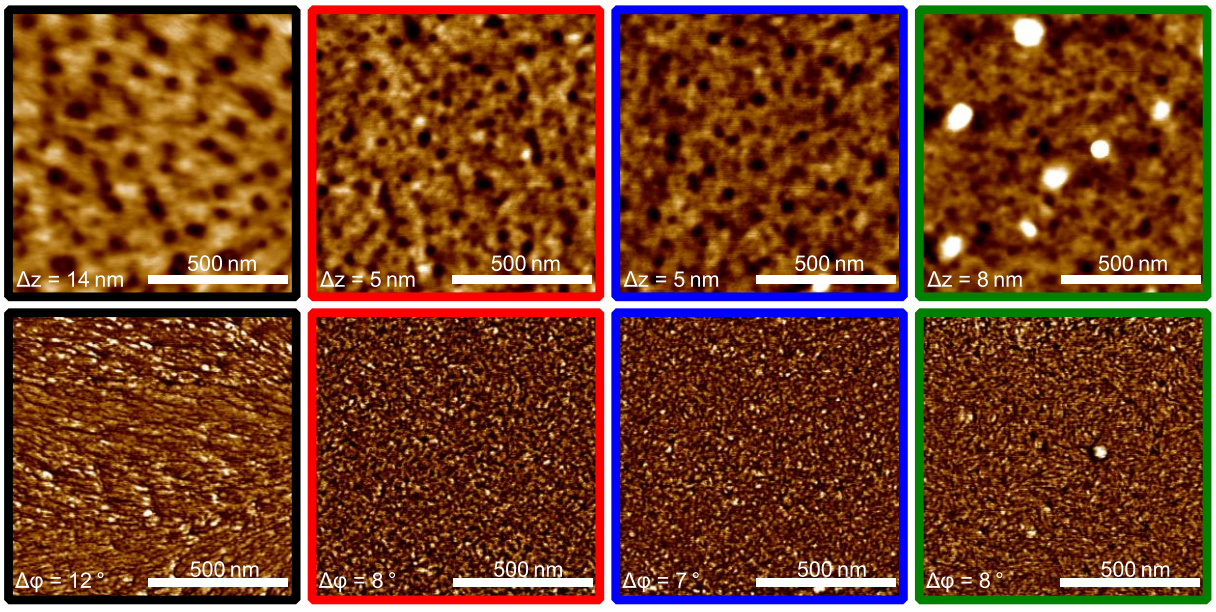

Figure S 8. AFM height and phase images obtained in tapping-mode of spin coated RR (black), RI(70:30) (red), RI(47:53) (blue) and RI(24:76) (green) thin films. Films were doped in TDAE vapor for 120 min at 35 °C.

Solution Doping with N-DMBI and Blade Coating

For solution doping and blade coating of P(NDI2OD-T_2) ($\overline{M_n}$ = 37 kg mol^{-1}, PDI = 3.2, $CHCl_3$ SEC calibrated vs. PS standards) the polymer was dissolved overnight in CB at 80 °C, c = 20 g l^{-1}. The solution was cooled to room temperature, N-DMBI was added (25 and 50 mol%, respectively) and the room temperature blend was blade coated on a blade coater (Erichsen Coatmaster 510, sample stage at 80 °C), a blade height of 100 µm and a speed of 1 mm s^{-1} on precleaned glass substrates (ultrasonication in ^{i}PrOH and acetone for 10 min each, followed by an oxygen plasma treatment for 10 min, 100 W). The blade coated films were immediately transferred into an inert atmosphere in a glove box and heated to 55 °C for 3 h.

For solution doping the procedure of blade coating had to be performed at room temperature. The optimized blade coating protocol with solution and sample stage temperatures of 80°C would have already induced the doping process, thus the P(NDI2OD-T_2)/N-DMBI blends were first blade coated from room temperature solutions and then the doping reaction was induced by heating the films at 55°C for 3 hours. Before inducing the doping reaction dichroic ratios can be determined to *DR* = 2.4 and 4.8 for doping amounts of 25 and 50 mol%, respectively (see Figure S 10). This is overall lower than in P(NDI2OD-T_2) blade coated homopolymer films and seems to be due to disturbance of the polymer alignment when N-DMBI is present. After inducing the doping reaction the anisotropy does not seem to change and a slight increase of a radical-anion band is visible at 489 nm comparable to what was observed in spin coated films. It was decided not to calculate dichroic ratios of the doped films due to the presence of the radical-anion band.

The conductivities were measured parallel and perpendicular to the blade coating direction and are denoted as $\sigma_{||}$ and $\sigma_{\perp}$, respectively (see also Figure 4). Values of $\sigma_{||} = 3.2 \cdot 10^{-3}$ and $\sigma_{\perp} = 1.2 \cdot 10^{-3}$ S cm^{-1} are obtained for samples doped with 25 mol% of N-DMBI, which results in an anisotropy factor of 2.7. These as well as all other conductivities and anisotropy

factors are summarized in **Erreur ! Source du renvoi introuvable.**. When the amount of N-DMBI is increased to 50 mol%, conductivity values of $\sigma_{\parallel} = 2.3 \cdot 10^{-3}$ and $\sigma_{\perp} = 5.7 \cdot 10^{-4}$ S cm^{-1} are observed, resulting in an anisotropy factor of 4.0. Interestingly, both dopant amounts of 25 mol% and 50 mol% result in values around $\sigma = 2 \cdot 10^{-3}$ S cm^{-1}. The anisotropy factors of 2.7 and 4.0 indicate a moderate difference between the conductivity parallel and perpendicular to the chain direction, but are lower compared to the anisotropies observed for example in electron mobilities in aligned films (around one order of magnitude or higher) by mechanical rubbing or blade coating.[15,20] This might be explained due to the disturbance of polymer chain alignment in presence of the dopant. Blend formation could be not fully homogeneous and therefore hindering a smooth and high alignment of the chains. Another reason for lower alignment in the films could be the fact that the blend solution was not heated at 80 °C after addition of N-DMBI.

Lower anisotropy in conductivity is also seen in lower dichroic ratios of 2.4 and 4.8 of N-DMBI/P(NDI2OD-T_2) blends. As observed for spin-coated films, no direct correlation between the molar ratio of polymer/dopant and the intensity of the radical-anion absorption can be made. This might be explained by the low miscibility of the dopant in the polymer matrix and thus different blend phase separation depending on the deposition conditions. Similar to spin-coated films, clustering of dopant on the surface of the film can be seen in all AFM images, independent of the amount of dopant used (Figure S 11).

Table S 1. Conductivity values and anisotropy factors for N-DMBI doping in anisotropic blade coated films.

	Doping with N-DMBI	
	25 mol%	**50 mol%**
$\sigma_{\parallel}$ / S·cm^{-1}	$(3.2 \pm 0.4) \times 10^{-3}$	$(2.3 \pm 1.4) \times 10^{-3}$
$\sigma_{\perp}$ / S·cm^{-1}	$(1.2 \pm 0.2) \times 10^{-3}$	$(5.7 \pm 3.4) \times 10^{-4}$
$\sigma_{\parallel} / \sigma_{\perp}$	2.7	4.0

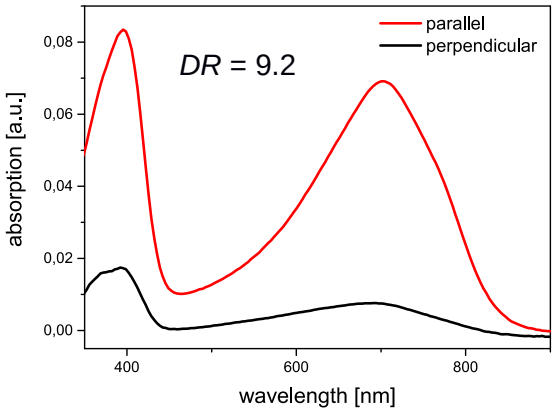

Figure S 9. Polarized absorption spectroscopy of blade coated P(NDI2OD-T_2) with $\overline{M_n}$ = 37 kg mol^{-1} and PDI = 3.2. The dichroic ratio is DR = 9.2.

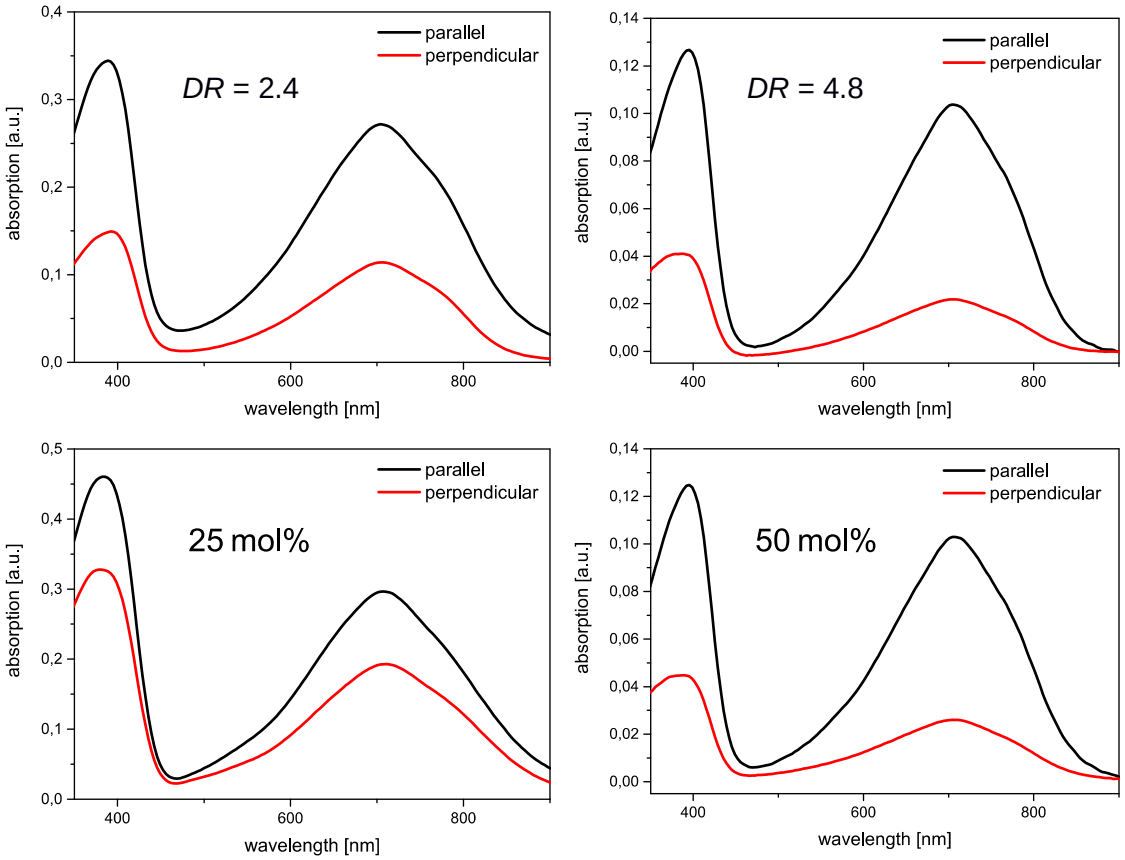

Figure S 10. Polarized absorption spectroscopy of blade coated P(NDI2OD-T_2)/N-DMBI blends with different amounts of N-DMBI. The top row corresponds to the absorption prior temperature treatment, the bottom row shows the absorption spectra after temperature treatment at 55 °C for 3 h.

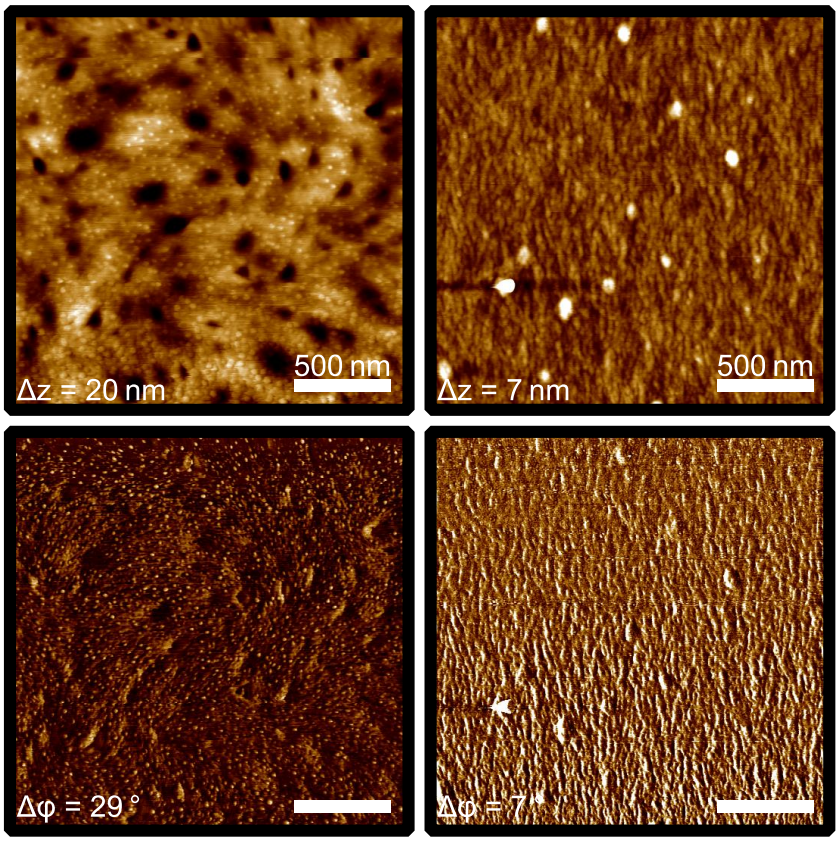

Figure S 11. AFM height (top) and phase (bottom) images obtained in tapping-mode of blade coated RR-P(NDI2OD-T_2)/N-DMBI (25 and 50 mol%) thin films. Films were temperature treated after blade coating to induce the doping reaction. The scale bars represent 500 nm.

Since an exact control over the amount of TDAE dopant is difficult to achieve by vapor doping, doping times were varied from 1 to 180 min and the conductivity was measured for different vapor exposure times (see Figure S 12). The graph shows the stepwise increase of the conductivity with increasing vapor doping time. After 1 min of vapor exposure, the conductivity was too low to be measured with our setup. 10 min of vapor doping lead to conductivities of around $3 \cdot 10^{-5}$ S cm^{-1}, saturating at around $3 \cdot 10^{-4}$ S cm^{-1} after 120 min. In literature it is proposed that short doping times around 60−90 s lead to the highest conductivities (around 10^{-3} S cm^{-1}) and further doping leads to a monotonic decrease of the conductivity.[54] These differences are likely due to usage of different doping chambers with different volumes and consequently different vapor concentrations. Thus, to increase the vapor pressure further, the temperature of the setup was increased to 35 °C in the following doping procedures.

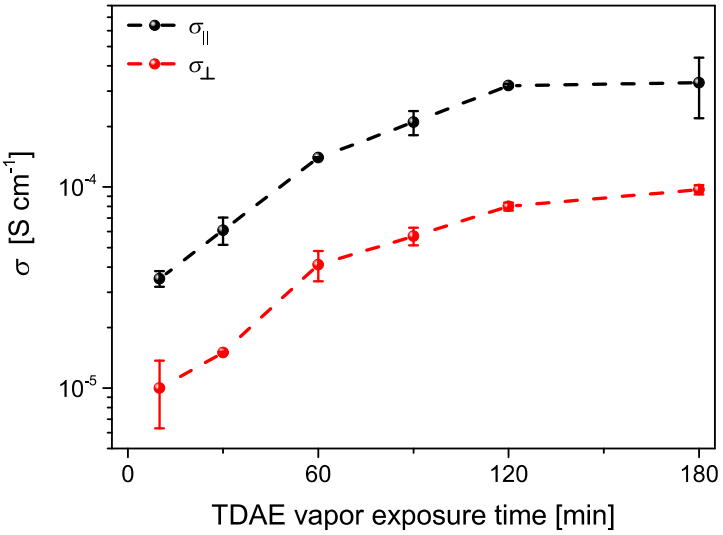

Figure S 12. Conductivity values after vapor doping of blade coated P(NDI2OD-T_2) films with TDAE for different doping times.

Table S 2. Conductivity values and anisotropy factors of blade coated P(NDI2OD-T2) films doped with TDAE in Figure S 12.

Doping with TDAE	**10 min**	**30 min**	**60 min**	**90 min**	**120 min**	**180 min**
$\sigma_{\parallel}$ / S·cm^{-1}	(3.5 ± 0.3) · 10^{-5}	(6.1 ± 0.9) · 10^{-5}	(1.4 ± 0.1) · 10^{-4}	(2.1 ± 0.3) · 10^{-4}	(3.2 ± 0.1) · 10^{-4}	(3.3 ± 1.1) · 10^{-4}
$\sigma_{\perp}$ / S·cm^{-1}	(1.0 ± 0.4) · 10^{-5}	(1.5 ± 0.2) · 10^{-5}	(4.1 ± 0.7) · 10^{-5}	(5.7 ± 0.6) · 10^{-5}	(8.0 ± 0.4) · 10^{-5}	(9.7 ± 0.5) · 10^{-5}
$\sigma_{\parallel}$ / $\sigma_{\perp}$	3.4	4.0	3.5	3.8	4.0	3.4

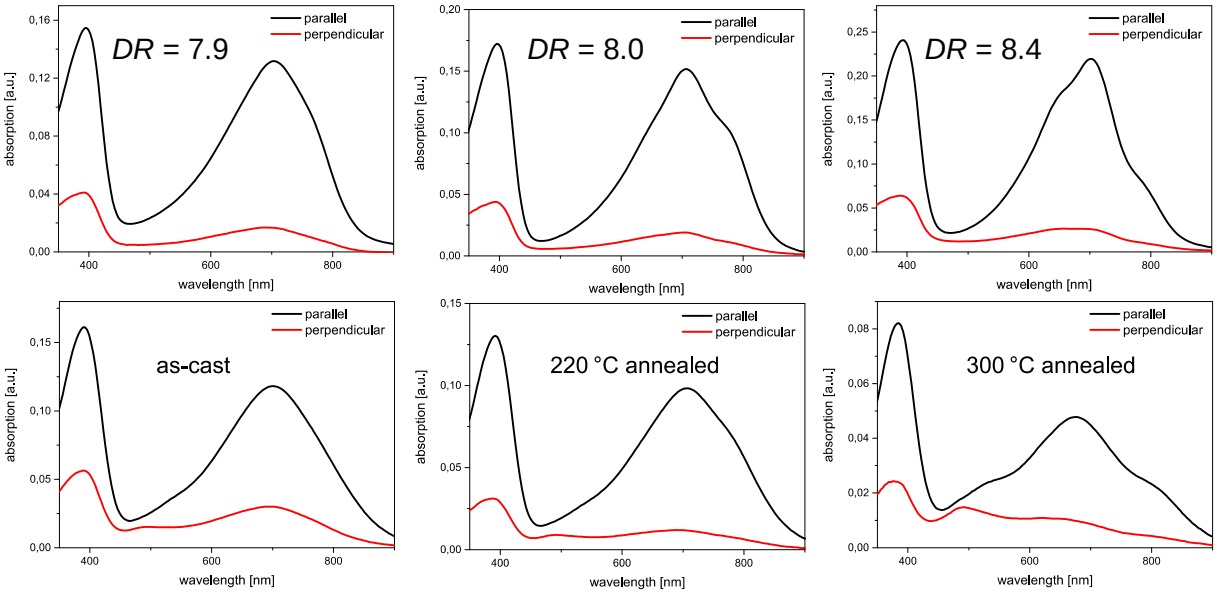

Figure S 13. Polarized absorption spectroscopy of blade coated P(NDI2OD-T_2) thin films. Films were annealed after blade coating at the indicated temperature. The top row shows the absorption prior doping, the bottom row shows the absorption of films exposed to TDAE vapor at 35 °C for 120 min.

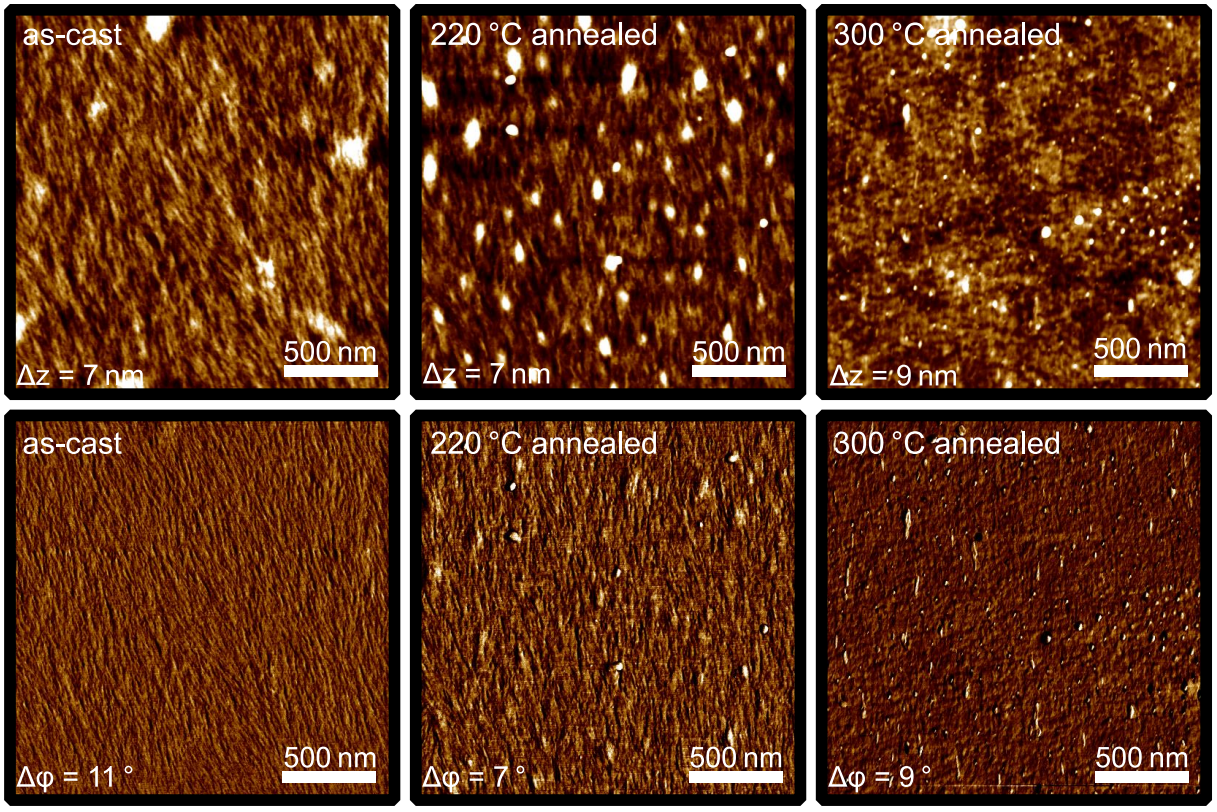

Figure S 14. AFM height (top) and phase (bottom) images obtained in tapping-mode of blade coated P(NDI2OD-T_2) thin films. Films were annealed after blade coating at the indicated temperature and exposed to TDAE vapor at 35 °C for 120 min. The scale bars represent 500 nm.

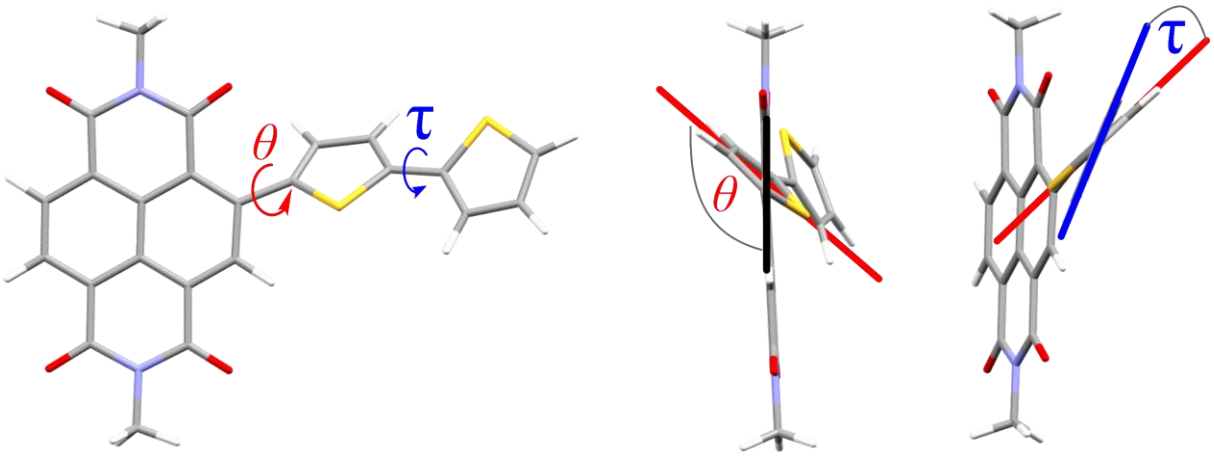

Figure S 15. Backbone dihedral angles are shown in the monomer structure, reproduced from (U)CAM-B3LYP/6-31G* optimized cartesian coordinates given in ref. [63]. The alkyl chains were replaced by methyl groups for computing reasons.

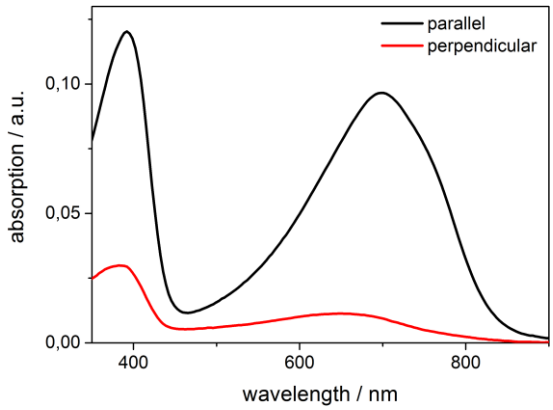

Figure S 16. Polarized absorption spectroscopy of a BC/300 °C P(NDI2OD-T_2) thin film exposed to TDAE vapor at room temperature for 120 min.

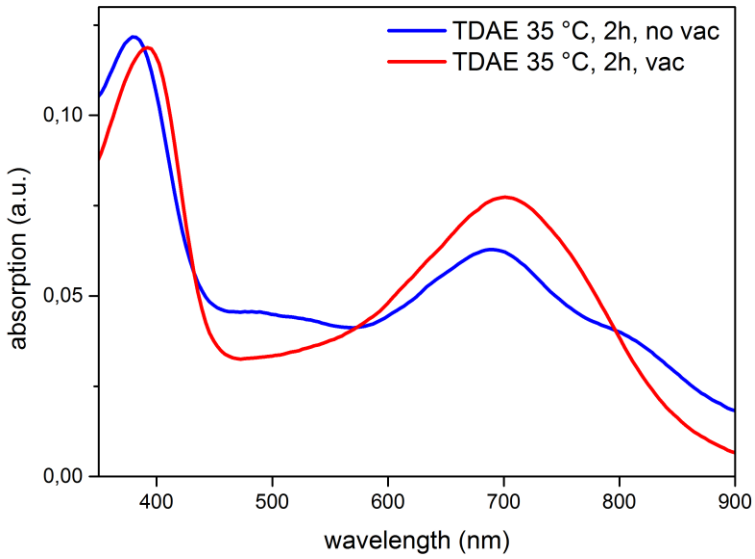

Figure S 17. Absorption spectroscopy of TDAE doped samples with and without vacuum treatment.

The UV–Vis data shown in Figure S 17 were recorded directly after vapor doping with TDAE, whereas all other data in the manuscript were recorded after conductivity measurements which included an electrode deposition step in vacuo. The spectrum after TDAE doping at 35 °C without additional vacuum (blue) shows a more pronounced radical-anion absorption as observed after the usual sample preparation including vacuum. If the sample is put in the vacuum of the evaporation chamber for 45 min, a decrease in the radical-anion absorption is visible (red) and corresponds to the spectra measured of the other samples in the manuscript. In terms of conductivity, both samples show values around 10^{-3} S cm^{-1}, which is in line with the values obtained in the manuscript. Thus, the films are partially dedoped when they are placed in vacuo.

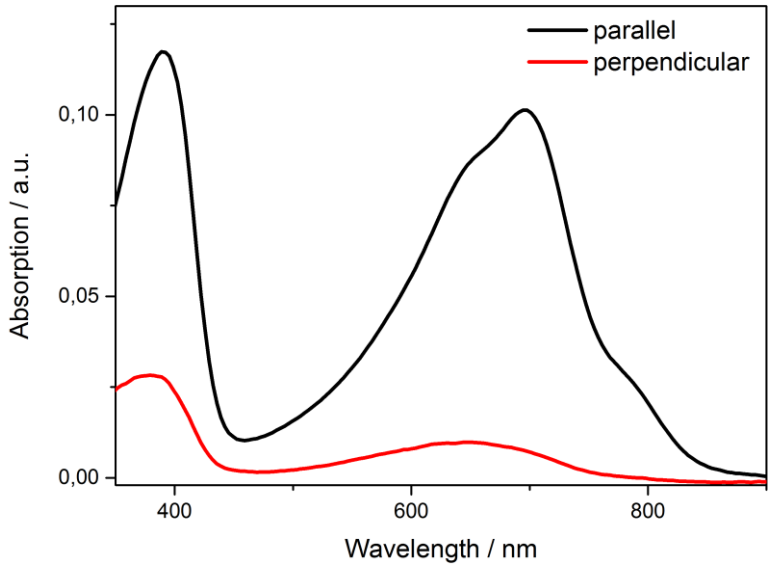

Figure S 18. Polarized absorption spectroscopy of a BC/300 °C P(NDI2OD-T_2) thin film exposed to TDAE vapor at 35 °C for 120 min and then again annealed at 300 °C.